MINUTES

OF THE TWENTY-FIRST EXPLOSIVES SAFETY SEMINAR

VOLUME I

HYATT REGENCY HOTEL

HOUSTON, TX

28-30 AUGUST 1984

SPONSORED BY

DEPARTMENT OF DEFENSE EXPLOSIVES SAFETY BOARD

ALEXANDRIA, VA

21st DoD EXPLOSIVES SAFETY SEMINAR
28-30 AUGUST 1984, HOUSTON, TEXAS (USA)

WINDOW PANES LOADED BY EXPLOSIONS

by

A. Harmanny, W. Karthaus and G. Opschoor

Prins Maurits Laboratory TNO
P.O.Box 45, 2280 AA Rijswijk
The Netherlands

1. INTRODUCTION

The Prins Maurits Laboratory TNO is interested in window-pane fracture by explosions for two reasons:

- Window-panes are the most vulnerable parts of buildings. So, for the safe distance to potential explosive sources the lower limit of window-pane fracture is very important.
- Because of their relative low breakage pressure window-panes often have a function as vents for a possible internal gas or dust explosion. In these situations the upper limit of the breakage pressure is important.

It is generally known that the pressures at which windows break vary widely and are difficult to predict.
This is partly because it is difficult to calculate the maximum stresses in a window-pane loaded by an explosion.
These mechanical problems fall into three groups:

- The dynamic response calculation.
  Often only the first normal mode of the pane is taken into account, but may be higher modes play an important part.
- The edge conditions.
  Normally panes are schematized as simply supported plates, but if the edges are not free to rotate some amount of clamping has to be taken into account.
- Membrane action.
  Especially for thin panes the behaviour is dominated by membrane action.

However, even if the stresses were known it is still difficult to predict the breakage pressure because the strength of the material glass is influenced by many quantities:

- Inhomogenities in the glass
- Scratches on the surface
- Age of the pane
- Single- or double-pane windows
- Thickness of the pane
- Duration of the loading
- Temperature of the glass
- Humidity of the surroundings.

To gain more insight into the mechanical problems strain-measurements have been performed on blast loaded windows. With the help of these measurements a calculation model for the maximum stresses has been developed. Besides, lots of tests have been carried out in order to determine the breakage pressure of panes with various dimensions. These tests provided the opportunity to verify the calculation model and to quantify the effect of thickness and area of the pane on its strength.

2. DETERMINATION OF STRAINS

The strain measurements were carried out on a square pane, with dimensions 420 × 420 × 5 mm. Strain gauges were cemented on both sides, perpendicular and parallel to both the diagonal and the mediane. The positions are sketched in Figure 1.

The pane was loaded by a shock wave with the help of the small PML 40 × 40 cm^2 square cross-section blast simulator. In order to gain more insight into the membrane action also tests were carried out on a pane made of some polycarbonate.

This material is much stronger and more flexible than glass, so the displacements of this pane were more than those of the glass-pane and therefore membrane action was more pronounced.

For comparison the strains were also calculated, assuming a simply supported Kirchoff-plate (without membrane action).

The plate with the axes of the coordinates used is sketched in Figure 2.

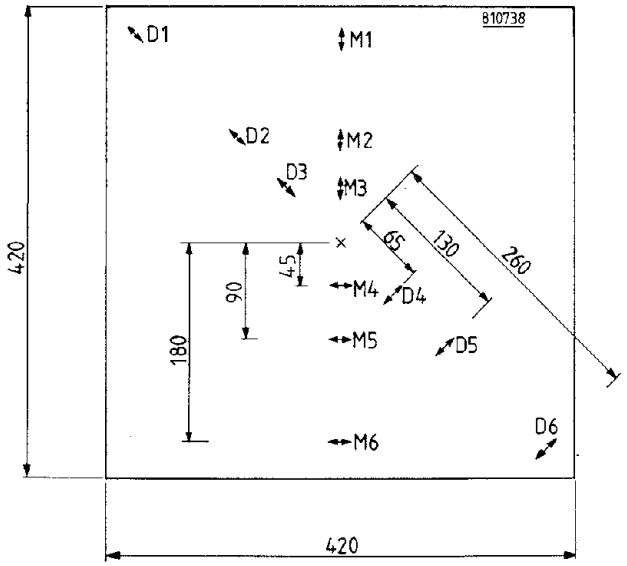

Figure 1.

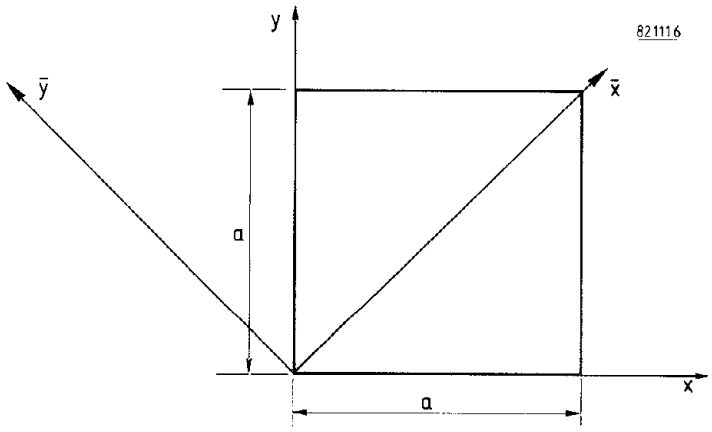

Figure 2. Plate with axes of coordinates.

The maximum displacements $\hat{z}$ under an even distributed static loading q is given by (ref. (1)):

$$\hat{z} = 0{,}00406 \quad \frac{q\, a^4}{D} \tag{1}$$

where D is the stiffness of the plate. To obtain the displacement under dynamic loading it had to be multiplied by a dynamic load factor (DLF) which is dependent on the duration t_+ of the shock wave and the first natural frequency ω of the plate.
This frequency is given by (ref. (2)):

$$\omega = \frac{2\pi^2}{a^2} \sqrt{\frac{D}{\rho h}} \tag{2}$$

where h is the plate thickness and ρ the density of the plate material.
The DLF, as a function of ωt_+, is given in Figure 3.

If it is assumed that only the first mode of the plate is important the displacement is given by:

$$z = \hat{z} \sin \frac{\pi x}{a} \cdot \sin \frac{\pi y}{b} \tag{3}$$

Now the bending moments can be found (ref. (1)):

$$M_x = M_y = \hat{z} \cdot D\,(1 + \nu) \frac{\pi^2}{a^2} \sin \frac{\pi x}{a} \cdot \sin \frac{\pi y}{b} \tag{4}$$

$$M_{xy} = \hat{z} \cdot D\,(1 - \nu) \frac{\pi^2}{a^2} \cos \frac{\pi x}{a} \cdot \cos \frac{\pi y}{b} \tag{5}$$

$$M_{\bar{x}} = M_x - M_{xy} \tag{6}$$

$$M_{\bar{y}} = M_x + M_{xy} \tag{7}$$

In these equations ν is Poisson's ratio.

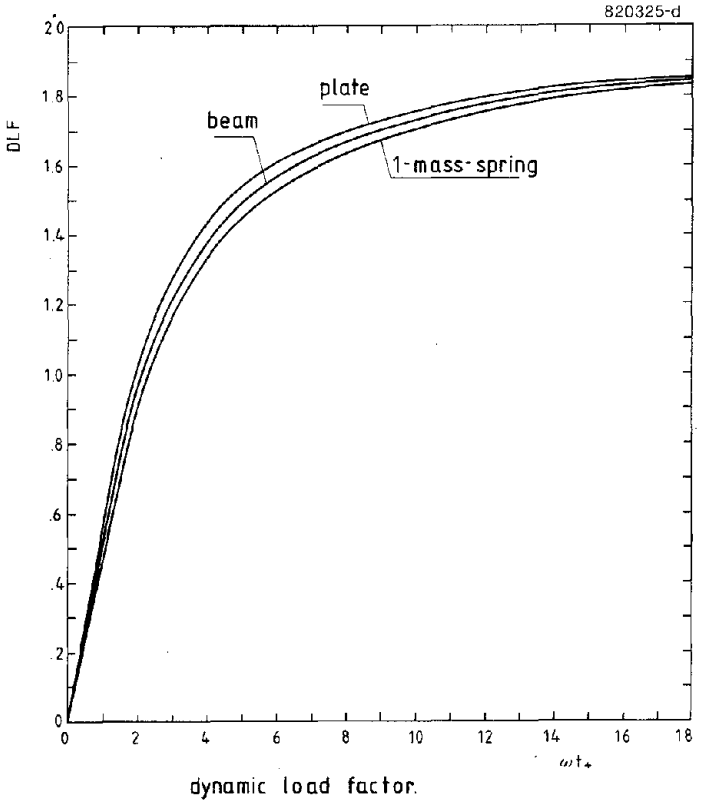

Figure 3.

Finally the strain ε follows from

$$\varepsilon = \frac{M}{1/6\ h^2 E} \tag{8}$$

In Figures 4 to 7 the calculated strain divided by the peak overpressure of the loading is compared with the measured maximum strains for the window-pane.

All the strains measured on the loaded side of the pane are multiplied by -1, so, if there is only bending, the strains measured on both sides should coincide.

From these Figures the following conclusions can be drawn:

- The assumption of a simply-supported plate is correct; Figures 4 and 5 show that there are no bending moments along the edges.
- Although the data are insufficient for the evaluation of the influence of higher modes it is clear that the first mode dominates the response.

- The effect of membrane action is obvious in the Figures: most of the strains measured on both sides do not coincide and are below the calculated strains.

  These phenomena tend to increase with increasing loading: because of the non-linear behaviour of membrane action the part of the loading carried by membrane action increases with increasing displacements.

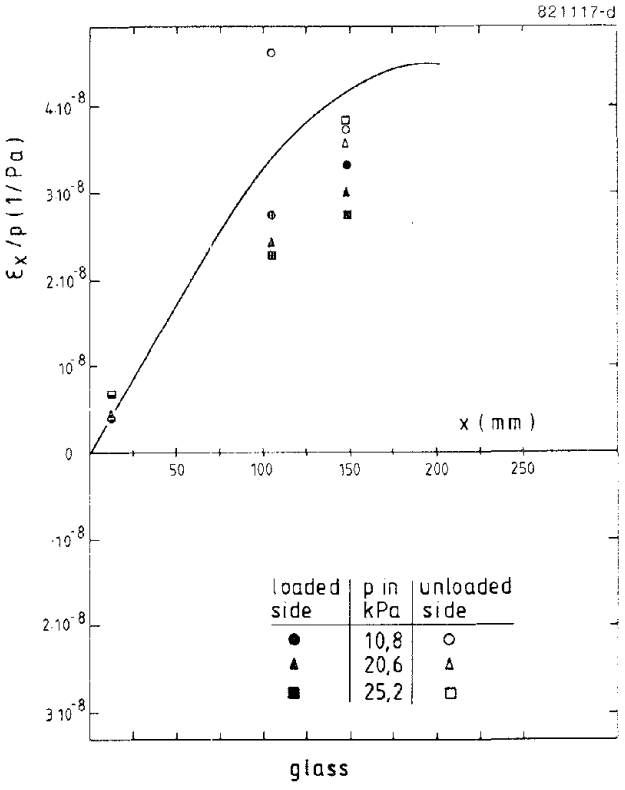

Figure 4. Strain parallel to the mediane.

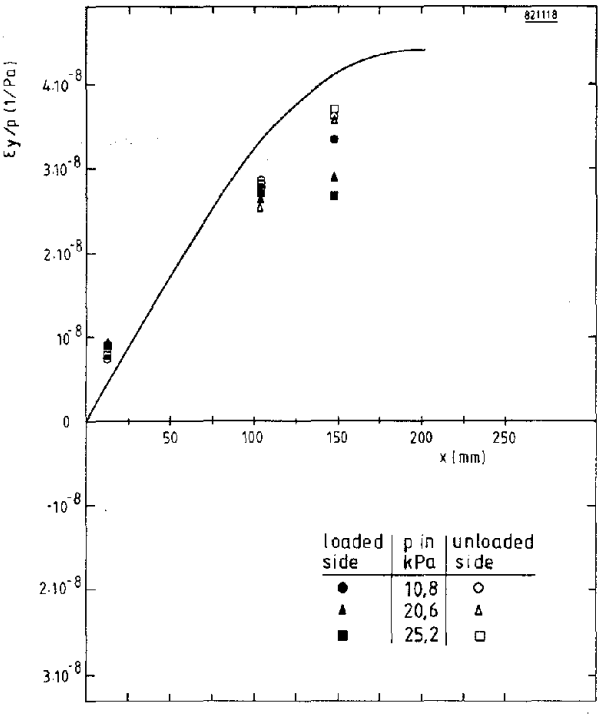

Figure 5. Strain perpendicular to the mediane.

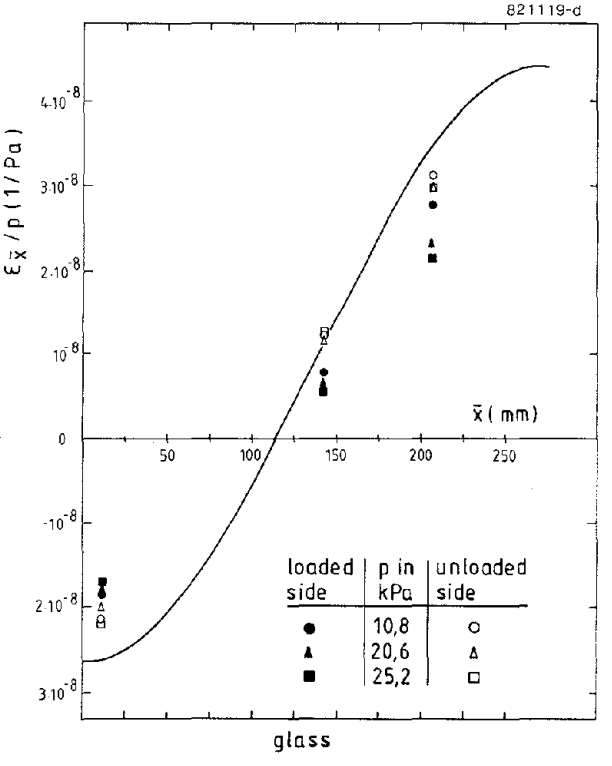

Figure 6. Strain parallel to the diagonal.

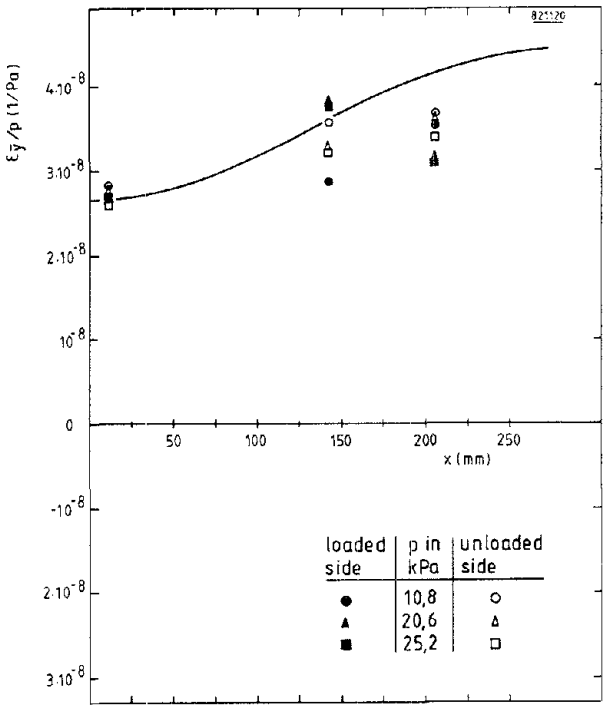

Figure 7. Strain perpendicular to the diagonal.

Figures 8-11 represent the strains for the polycarbonate in the first three loading steps. The conclusions are the same as for glass, but the influence of membrane action is even more pronounced.

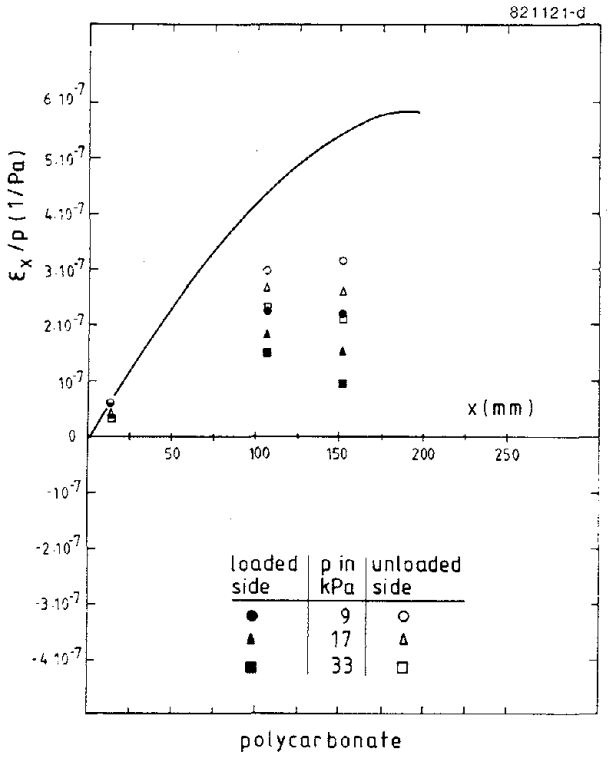

Figure 8. Strain parallel to the mediane.

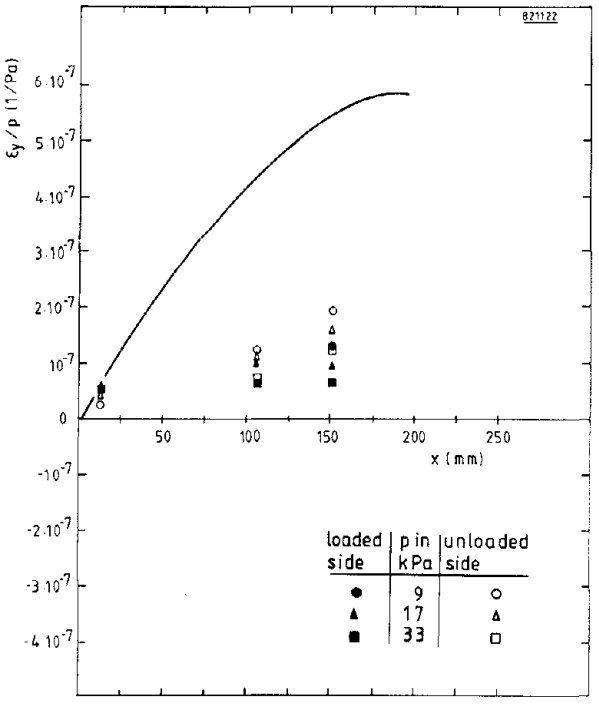

Figure 9. Strain perpendicular to the mediane.

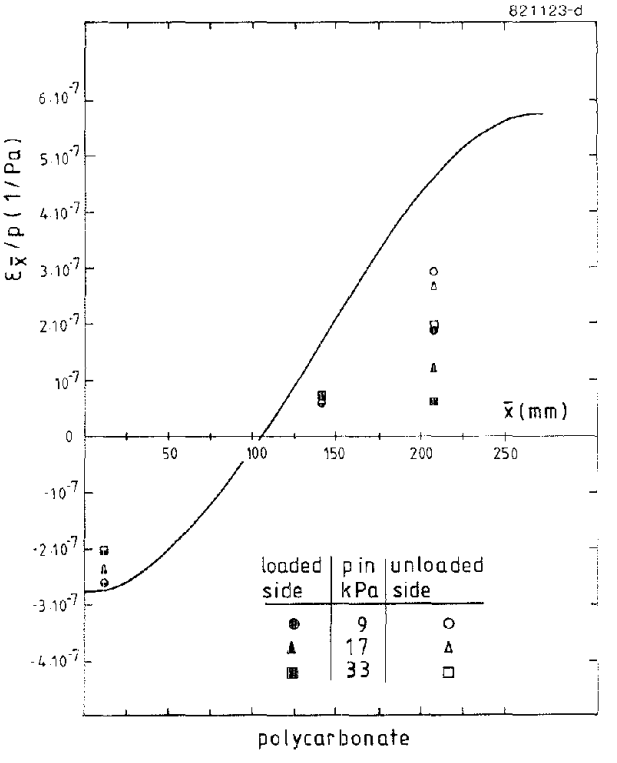

Figure 10. Strain parallel to the diagonal.

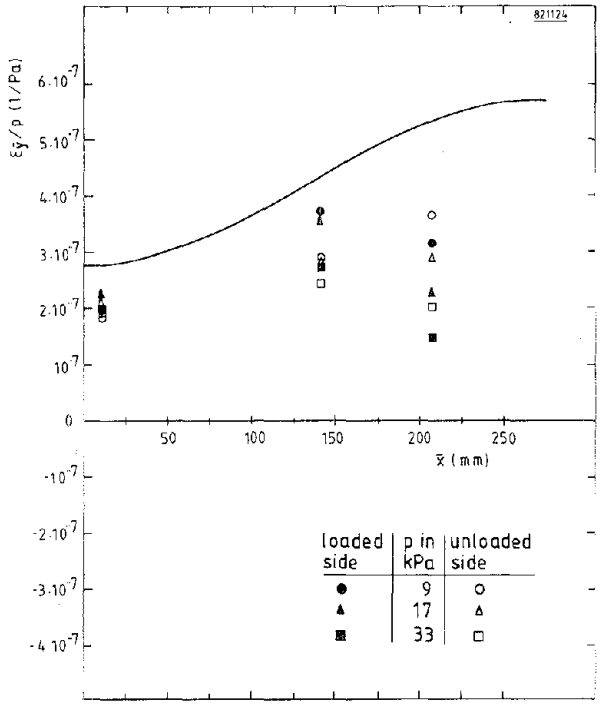

Figure 11. Strain perpendicular to the diagonal.

3. DERIVATION OF CALCULATION MODEL

From the strain measurements it is clear that by neglecting membrane action the strains are greatly overestimated.

It is very well possible to calculate the strains in a square (or rectangular) membrane that is fixed along the edges (ref. (1)).

Although the combination of bending and membrane action is much more complicated some investigators have developed approximate formulae that take into account both bending and membrane action (ref. (3) and (4)) by assuming fixed edges.

However, the strain measurements clearly show that there are no membrane stresses perpendicular to the edges (Figs. 4 and 8). This means that these edges are free to translate inward and that the assumption of fixed edges will give an overestimate of the membrane action.

Unfortunately it is impossible to give an analytic solution of membrane action in rectangular plates with edges that are free to move. There is a possibility however to obtain results in each specific situation with the help of finite-element-methods.

For the drafting of a new Dutch Building code on window-panes lots of finite-element-calculations have been performed. One of the conclusions that could be drawn from the results is, that the point in which the stresses are maximal, moves from the centre of the pane, along the diagonal, to the corners. This is in agreement with the strain measurements: the relative strains in the corners remain about constant under uncreasing loading, while all the other relative strains decrease. Figs. 6, 7, 10 and 11 with $\bar{x} = \bar{y} = o$). Therefore it is rational that these strains will finally become decisive.

In order to check whether the relative strains in the corners also remain constant under very high deformation and are thus not influenced by membrane action, in Figure 12 the relation is given between these strains and the peak overpressure of the loading for the polycarbonate.

In the plot also the theretical relationship is drawn.

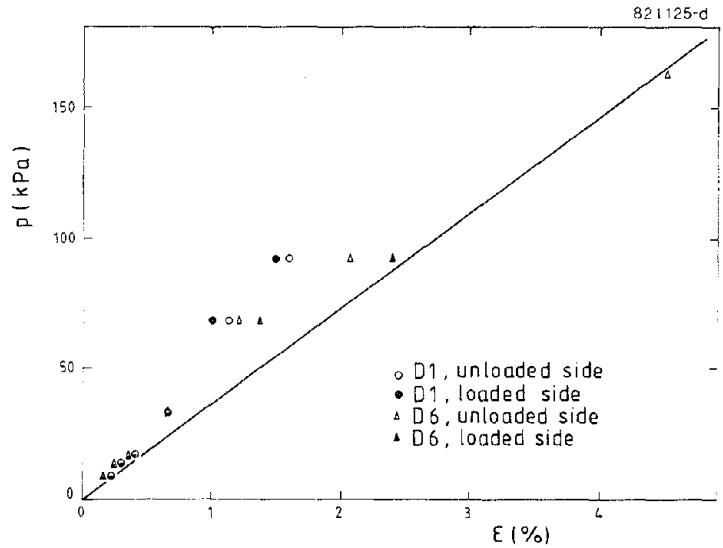

relation between overpressure and strains near the corner of a pane.

Figure 12.

For very high loadings there appears to be some influence of membrane action, but it is clear that by assuming a simply-supported Kirchoff-plate the maximum strains in the corners can be predicted quite accurately.
Although the measurements have been carried out on a square plate, it is to be expected that rectangular plates will behave in the same way.
So, for rectangular plates the maximum stresses are the bending stresses in the corners if the deflections are big enough.
These stresses are given by:

$$\sigma = 51 \cdot \alpha \frac{q}{h^2} \cdot \frac{a^3}{b} \qquad (9)$$

where b is the greater span and α a coefficient dependent on the b/a ratio. Numerical values for α are given in Table 1 (ref. (1)).

TABLE I. Numerical values for α.

b/a	$\alpha(\times 10^{-3})$	b/a	$\alpha(\times 10^{-3})$
1,0	4,06	1,6	8,30
1,1	4,85	1,7	8,83
1,2	5,64	1,8	9,31
1,3	6,38	1,9	9,74
1,4	7,05	2,0	10,13
1,5	7,72	3,0	12,23

It appears that α is more or less directly proportional to b/a, so eq. (9) can be approximated by:

$$\sigma = 0{,}225\, q\, \frac{a^2}{h^2} \qquad (10)$$

4. VALIDITY OF THE MODEL

Eq. (10) is only valid if the deflections are big enough. So, it is necessary to determine whether the equation may be used. From ref. (1) it can be derived that, as an approximation, the influence of membrane action relative to bending is determined by the factor $C \cdot \frac{\hat{z}^2}{h^2}$.

Coefficient C generally depends on the edge conditions, Poisson's ratio and the length-to-width ratio b/a of the plate.
The edge conditions are the same for all panes. From the strain measurements it can be found that for both the glass and the polycarbonate pane the strains in the corners become decisive at about $\hat{z}/h = 6$.
So, only the effect of b/a on C has to be quantified. Increasing the b/a ratio has two aspects:

(a) The effect of membrane action decrease: for large b/a ratios there is no membrane action.

(b) The bending stresses near the centre increase much more than those near the corners.

Both aspects will result in an increase in the critical $\hat{z}/h$ ratio.

The influence can be quantified as follows:

(a) A formula in ref. (5) suggests that C is about proportional to $(a/b)^2$, so the critical $\hat{z}/h$ would be proportional to b/a.

(b) As the stresses in the centre are almost proportional to b/a, while those in the corners are almost constant, the critical $\hat{z}/h$ would be proportional to $(b/a)^{1/2}$.

On aggretate the critical value of $\hat{z}/h$ will be proportional to $(b/a)^{3/2}$.
This is visualised in Figure 13.

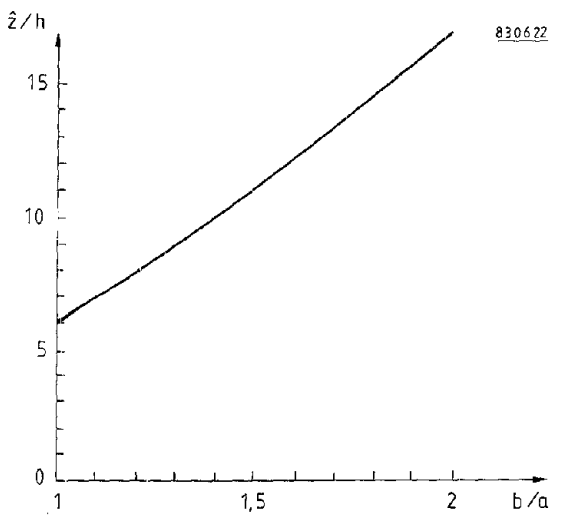

critical value of max displacement as a function of length-width ratio

Figure 13.

The displacement $\hat{z}$ for rectangular plates follows from:

$$\hat{z} = \alpha \cdot \frac{q\, a^4}{D} \qquad (11)$$

Because of the uncertainties in the reasoning for the critical value of $\hat{z}/h$ it is advisable to use the result only for b/a ratios up to 2.
In those situations where $\hat{z}/h$ is smaller than the above given critical value, eq. (10) may not be used, but membrane action may already be considerable. Therefore it is advisable to interpolate linearly between the normal bending stress in the centre of the pane and the stress given by eg. (10).
This leads to:

$$\sigma = f \cdot 0{,}225 \cdot q \frac{a^2}{h^2} \qquad (12)$$

and the correction factor f follows from:

$$f = 1 + 1/9 \left[(\hat{z}/h)_{cr} - \hat{z}/h \right] \qquad (13)$$

where $(\hat{z}/h)_{cr}$ is the critical value given by Figure 13.

5. EVALUATION OF BREAKAGE TESTS

The breakage pressures found for 220 panes have been analysed with the calculation model derived earlier.
Attention has been given to the influence of:

(a) length-to-width ratio
(b) thickness of the pane
(c) area of the pane
(d) application of double panes.

(a) The panes in the tests had length-to-width ratios from 1, 1,5 or 2. Application of the model compared favourably with the actual results.

(b) The thicknesses of the panes tested ranged from 1,3 to 6,5 mm; in all there were 8 different thicknesses.
From the properties of glass it can be explained that the strength will increase with decreasing thickness (ref. (6)). When the strength of a pane with a thickness of 6 mm is assumed to be one, the relative strength of other thicknesses are given in Figure 14.

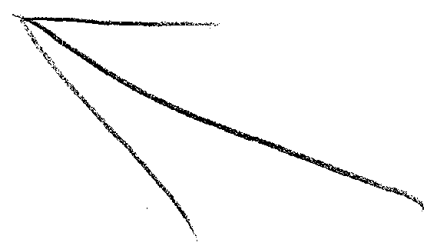

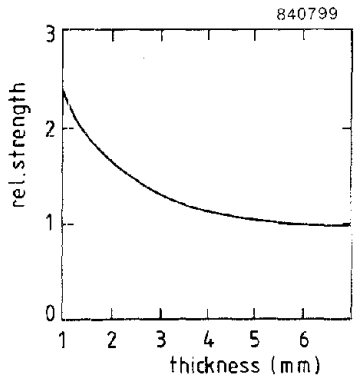

effect of thickness on tensile strength.

Figure 14.

(c) The panes tested had areas of 0,16, 0,18, 0,32 and 1,8 m^2. The later were tested in the 2-m blast simulator, Figure 15.

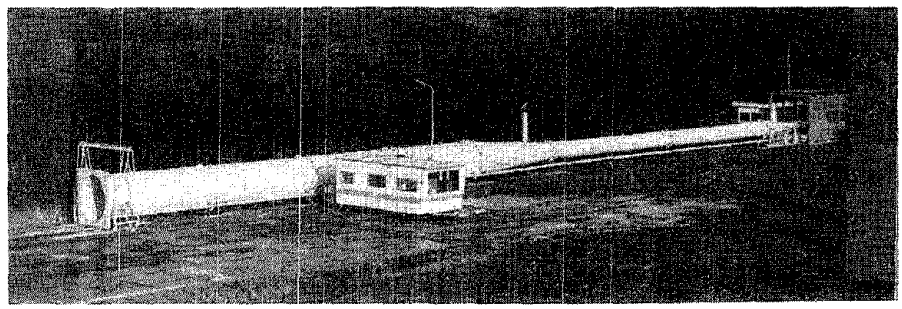

Figure 15. Overview of the 2-m PML blast simulator.

Since with increasing area also the chance of a severe scratch being present increases, the strength will decrease with increasing area. Ref. (7) states on the basis on statistics that by increasing the area by a factor of 10, the strength will be reduced by one third. This is in agreement with the tests.

(d) The breakage pressure of double panes can be calculated by assuming that both panes always move together.
So, when both panes have equal thickness, the breakage pressure will be double that of a single pane.
However, the strength will reduce by 10 percent, for the same reasons as under (c).

The strength of a pane with a surface area of about 2 m^2 and a thickness of 6 mm, loaded by an explosion, is about 65 MPa with a standard deviation of 20 percent.

6. CONCLUSIONS

It is possible to calculate the maximum stresses in blast-loaded, rectangular window-panes, with the help of the stresses in the corner of a simply supported plate under pure bending.

A value for the strength of glass has been established that may be adjusted for changes in pane area and thickness.

REFERENCES

(1) S.P. Timoshenko, S. Woinowsky-Krieger
Theory of plates and shells.
Mc Graw-Hill, 1959.

(2) S. Timoshenko, D.H. Young, W. Weaver
Vibration problems in engineering.
John Wiley and Sons, 1974.

(3) E. Abrahamsson
Blast loaded windows.
18th Explosive Safety Seminar, 1978.

(4) D.K. Pritchard
Breakage of glass windows by explosions.
Journal of Occupational Accidents, 3 (1981) 69-85.

(5) F. Rischbieter
Rechnerische Untersuchungen zur Schadenanalyse bei Gasexplosionen.
Battele Institut, Frankfurt, 1981.

(6) A. Harmanny
Glass Hazard.
Europex symposium: Explosion protection in practice.
Antwerp, 1984.

(7) W.G. Brown
A load duration theory for glass design.
Lecture for the International Committee on Glass.
Toronto, 1969.

VEHICLE OVERTURNING VULNERABILITY FROM AIR BLAST LOADS

R.R. Robinson*, H. Napadensky* and A. Longinow**

Introduction

The overturning response of an armored personnel carrier to air blast loads derived from a nuclear blast environment is presented herein. The vehicle considered is representative of an armored personnel carrier (APC). The orientation of the vehicle is side-on to the air blast shock front. It is assumed that either there is sufficient friction at the vehicle/ground surface interface or that the downwind wheels are chocked so that there is no translation at the downwind wheels, i.e., the roll over point. In addition, the vehicle is assumed to behave as a rigid body. That is, the suspension systems is taken as rigid, so that the wheels and axles rotate in unison with the body. It can be shown that this assumption slightly overestimates the overturning resistance of vehicles with suspension systems. For a stiff suspension system, such as that of the APC, the rigid body behavior assumption is justified.

The air blast loads are obtained by considering the diffraction and drag forces, acting on a series of interconnected rectangular blocks positioned in space which represent the aerodynamic model of the vehicle. The separate block loads at any time step are summed-up to obtain the total load history acting on the rigid body, single degree of freedom dynamic model. The only motion possible for this analysis is rotation about the rollover point. The effect of overturning restraint systems has been included in the analysis by incorporating a perfectly plastic vehicle to ground connection on the upwind side of the vehicle. The results presented give the threshold nuclear environment that just causes overturning. The threshold environment is given in terms of a peak overpressure corresponding to a weapon yield. Results are presented for a range of weapon yields from 1KT to 1MT.

*IIT Research Institute, Chicago, Illinois
**Illinois Institute of Technology, Chicago, Illinois

Method of Analysis

A computer program (OVRTRN) was used to numerically determine the overturning potential of an airblast load applied to a vehicle. The program incorporates the recently developed Ballistic Research Laboratory BLOP program to obtain the airblast loading on the vehicle.

The OVRTRN code can be used to evaluate both the reflected pressure loading and the drag loading that occurs from the dynamic pressure. The reflected pressure loading can be optionally included as an impulse load which imparts an initial velocity to the vehicle. It is also possible to evaluate the influence of nonlevel terrain since an initial angle (from the horizontal) of the ground surface can be specified by the user. In addition, the effect of a moving vehicle can be approximated by the application of a lateral load to the center of mass to simulate the centrifugal loading of the vehicle traveling around a curve. This feature can also be used to study the effect of perfectly plastic restraints connected between the vehicle and the ground. The overturning resistance provided by the restraint or tie downs can be easily related to a centrifugal force applied to the center of mass toward ground zero.

The numerical integration solution procedure of the equations of motion employed in the OVRTRN program is an explicit, central difference technique. The solution is automatically terminated if the vehicle rotation exceeds the instability rotation angle. Instability is assumed to occur when the center of mass rotates to a point directly over the rollover point. It is noted that for the case where restraints are included or there is a centrifugal force toward ground zero that larger rotations can occur before tipover. For this case, it is necessary to continue the solution further to establish whether tipover occurs.

The technique used to analyze the vehicle for overturning was to assume that the complete system is a single rigid body incapable of sliding motion. This assumes that the coefficient of friction between the wheels and the ground surface is sufficiently high and that any lifting forces acting on the vehicle are negligible compared to its weight. This latter assumption assures that there will be a nontensile vertical interface force (reaction) between the vehicle and the ground surface.

Figure 1 illustrates an APC subjected to side-on blast loading and the only degree-of-freedom possible, which is the rotation (θ) about the downwind track/ground surface interface, Point A. The time dependent blast load resultant lateral force is denoted by F(t). The height or point of application of the blast load, h(t), is also time dependent since some of the smaller components parts (e.g., wheels) which are modeled as rectangular boxes in the BLOP code will have shorter duration diffraction phase loading than other components. However, after the diffraction phase loading is over, the point of application of the resultant blast load will not appreciably change. The angle, θ, represents the rotation of the rigid body vehicle model from its initial position θ_o. If the vehicle is on level ground, then θ_o = 0.0. It is also assumed that the rigid body is initially at rest ($\dot{\theta}_o = 0$); however, there is an option to provide for both nonzero initial values of θ_o and $\dot{\theta}_o$. An initial nonzero θ_o would represent a rigid body on nonlevel ground and nonzero $\dot{\theta}_o$ can be used to represent the short duration reflected pressure and/or diffraction phase loading impulse. An initial value of $\theta_o > o$ indicates that the ground slopes away from ground zero and this would increase the vulnerability of the vehicle to overturning.

The effect of centrifugal loading to simulate vehicle travel at constant velocity around a curve or the equivalent overturning resistance offered by a perfectly plastic restraint is modelled by the application of a horizontal force resultant, γW, applied laterally to the center of mass as indicated in Figure 1.

The equation of motion that governs the time dependent rotation of the rigid body is

$$I_A \ddot{\theta} + M_R\{\theta\} = M_F\{t,\theta\} \qquad (1)$$

where I_A = second moment of mass of the rigid body about point A

$M_R\{\theta\}$ = restoring moment = $Wx\{\theta\} + \gamma Wy\{\theta\}$ (2)

$M_F\{t,\theta\} = F\{t\} \cdot H\{t,\theta\}$ = air blast overturning moment (3)

$x\{\theta\}$ = rotational dependent horizontal distance from point A to the center of mass

$y\{\theta\}$ = rotational dependent vertical distance from point A to center of mass

W = total weight of rigid body

$F\{t\}$ = time dependent horizontal force acting on rigid body

$H\{t,\theta\}$ = time and rotation dependent vertical location of $F\{t\}$ from point A.

The parameter $H\{t,\theta\}$ can be used to compute the overturning moment, M_F, rather than merely the BLOP code computed $h\{t\}$ for the following reason. As the rigid body rotates, it is reasonable to assume that the BLOP code computed overturning moment (which is the lateral force times to height to its point of action) will be increased from at least two sources: (1) lift forces will be produced on the underside of the rigid body, and (2) the drag area will be increased (at least for the initial rotations). In order to approximately account for the rotational increase to the overturning moment, it can be assumed that the $h\{t\}$ variable should be modified to produce $H\{t,\theta\}$ which is used in Equation (3) to compute the overturning moment. The procedure used assumes that the location of the center-of-pressure (C.P.) is a function of the rotation (θ), viz,

$$H\{t,\theta\} = h\{t\}\cos\theta + \sin\theta \qquad (4)$$

The restoring moment is the first moment of the vehicle weight gravitational vector, W, and the horizontal force, γW, about point A. Initially, the location of the W and γW vectors for level ground is $x = x_o$ and $y = y_o$, respectively. The distance from point A to the center of mass is

$$R = x_o^2 + y_o^2 \qquad (5)$$

The second moment of mass is computed from

$$I_A = I_o + Wr^2/g \qquad (6)$$

where I_o = moment of inertia about center of mass = Wr^2/g

r = radius of gyration

Armored Personnel Carrier Analysis

The basic parameters used in the overturning analysis of an APC are

W = 24,000 lb (weight)

r = 37.54 in. (Radius of Gyration)

x_o = 50 in.

y_o = 39 in.

$w = 100$ in.

The critical instability angle, θ_c, which is the angle at which the center of gravity is directly above point A, is given by

$$\theta_c = \tan^{-1}(x_o/y_o)$$
$$= 52 \text{ deg.}$$

Even though the OVRTRN program has the capability to increase with rotation (θ) the BLOP code computed vertical location of the center of pressure, this option has not been used for this analysis. A total of 16 different blocks were used to define the aerodynamic model of the APC as shown in Figure 2. The majority of these blocks were used to model the ten (10) track wheels. The hull was modeled with five (5) blocks and one (1) additional block for the gun and hatch at the top of the vehicle.

The typical angular response of the vehicle is shown in Figure 3. These results are for a weapon yield of 10 KT. The critical overpressure for this yield for the case where there is no tie-down restraint is $p_o = 14.4$ psi. The response for slightly higher (14.5 psi) and lower (14.3 psi) overpressures is also shown in Figure 3. For the higher overpressure level, the critical angular rotation of $\theta_c = 52$ degrees is reached at $t = 1.44$ sec and the angular velocity is 13.9 degrees/sec. The solution was terminated at this time; however, the angular displacement and rotation would increase rapidly after this time since the gravity vector also contributes to the overturning moment.

The vulnerability curve for the APC is shown in Figure 4. Four curves are shown therein representing the overturning vulnerability for the case where there is no external tie-down restraint ($\gamma = 0$) and also three (3) magnitudes of restraint, i.e., $\gamma = 0.1$, 0.25 and 0.50. It is seen that for high weapon yields, the restraint is not as effective at increasing the overturning hardness as it is at lower weapon yields. If the tie-down system was oriented at 45 degrees with the ground surface and located at a point near the top of the hull (70 inches above the ground), the required total tie-down force of the restraint system would be

$$F = \frac{\sqrt{2}\,(39)}{100 + 70}\,\gamma W$$
$$= 7785\,\gamma$$

Thus for a restraint parameter of $\gamma = 0.5$, the tie-down system would have to supply a plastic resistance force of 3,893 lbs. This is not an unreasonable value that could be obtained from a rapidly deployed light gage cable and anchor system.

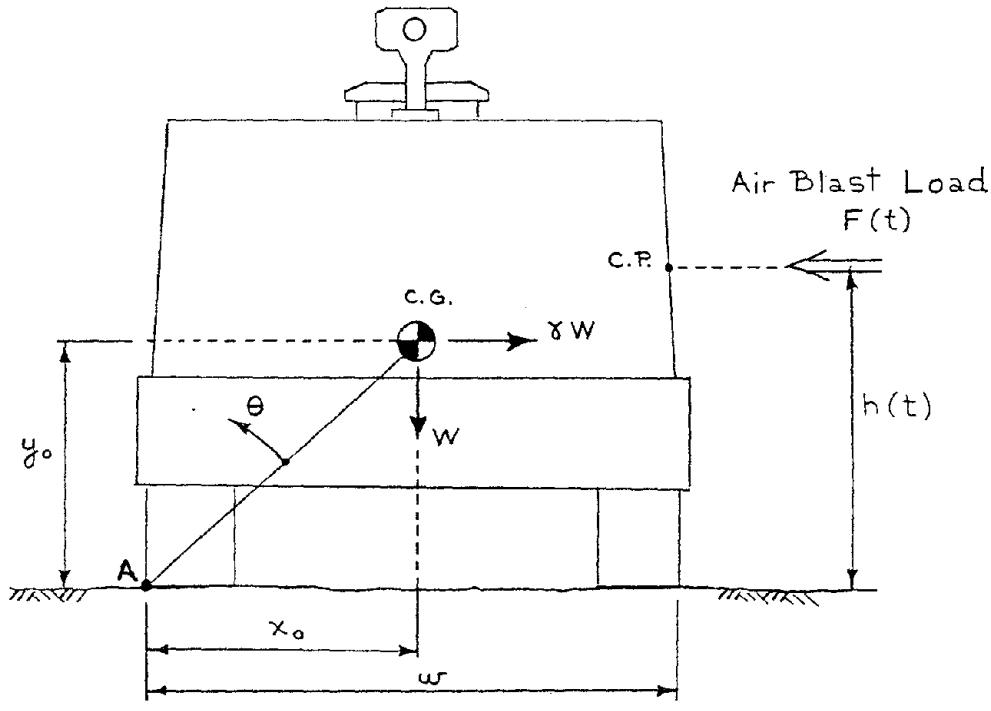

Figure 1. Rigid Body Overturning Model

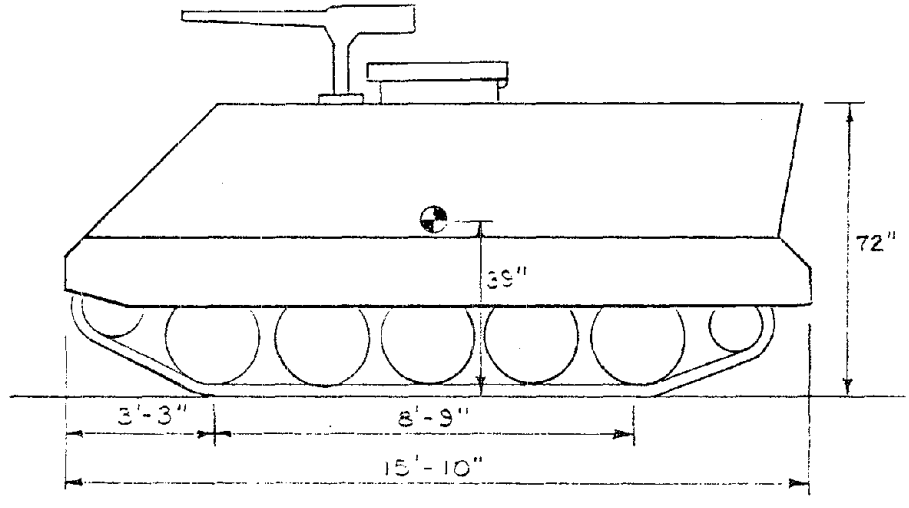

Side View

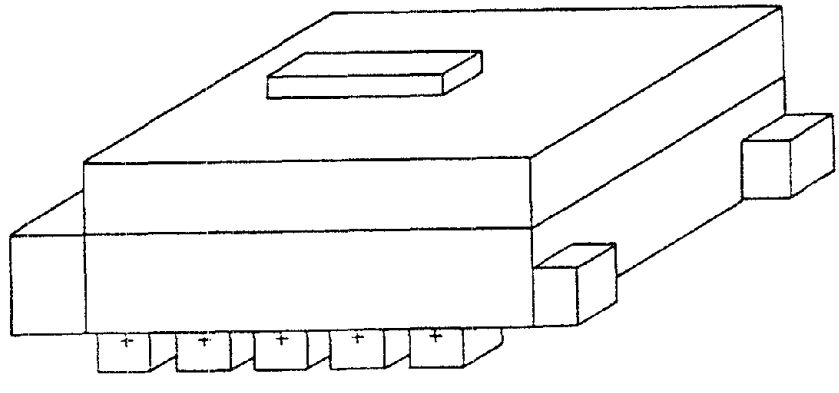

Aerodynamic Model

Figure 2. Armored Personnel Carrier

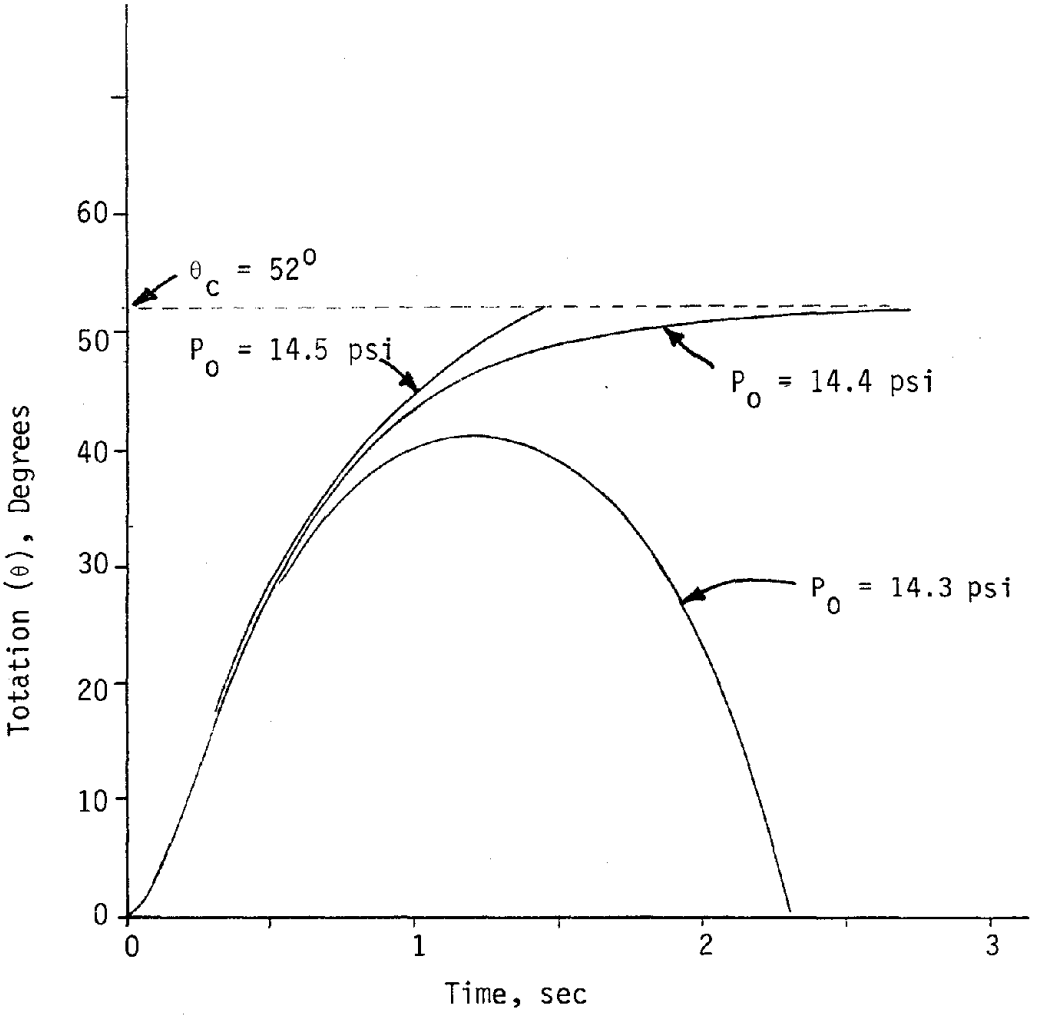

Figure 3. Rotational Variation for 10 KT Weapon Yield and Various Peak Overpressures (P_o)

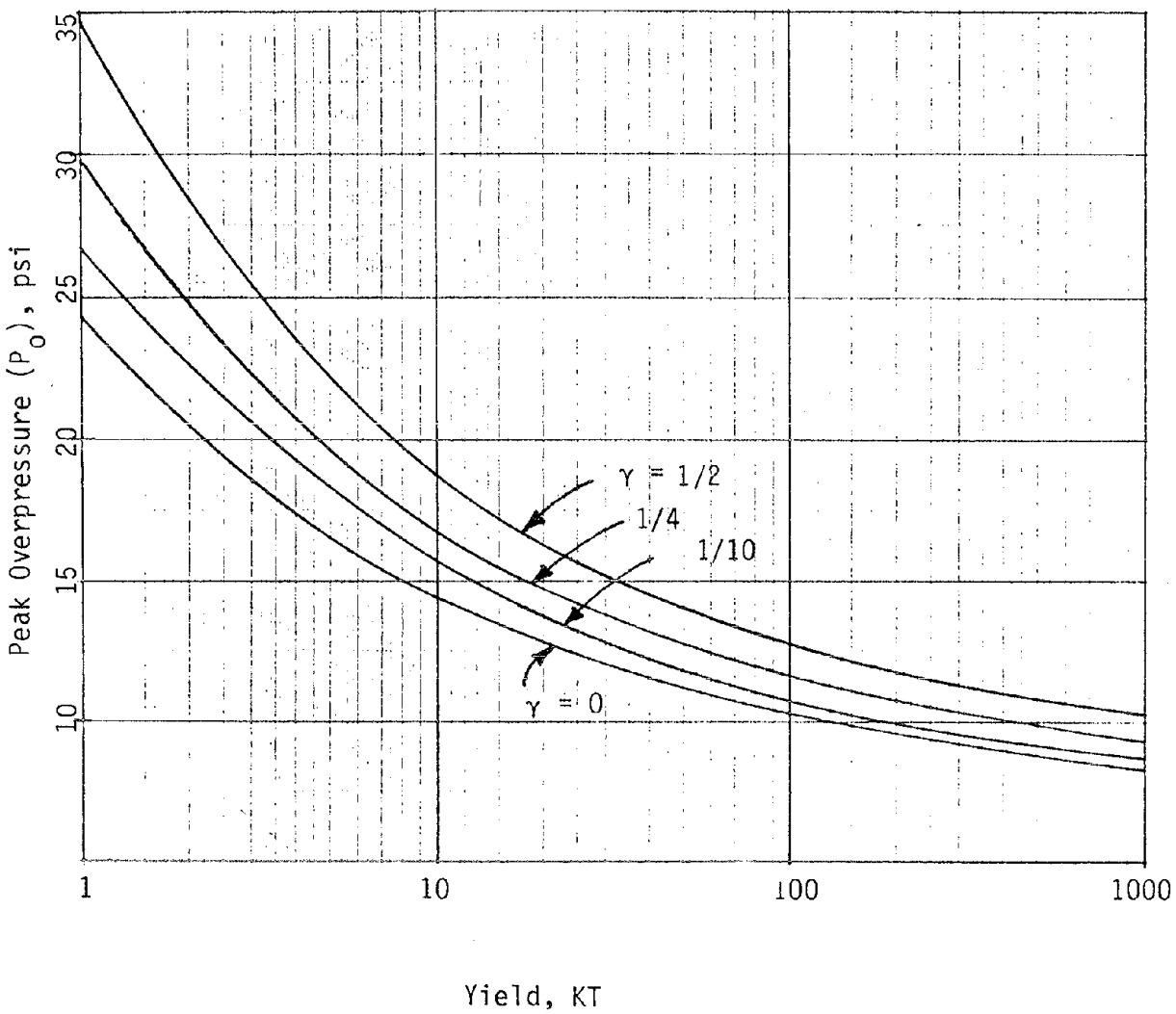

Figure 4. APC Overturning Vulnerability for Various Restraint Parameters (γ)

REFLECTED OVERPRESSURE IMPULSE ON A FINITE STRUCTURE

by
George A. Coulter
Charles N. Kingery

U.S. ARMY MATERIEL DEVELOPMENT AND READINESS COMMAND
U.S. ARMY BALLISTIC RESEARCH LABORATORY
ABERDEEN PROVING GROUND, MD 21005

ABSTRACT

This paper presents the effect of angle of incidence of the shock front on reflected impulse loading on a finite structure is presented in this paper. Impulse reflection factors have been developed for angles of incidence from zero to ninety degrees. Reflected impulse on a finite structure is much less than reflected impulse on an infinite plane because of the unloading due to rarefaction waves propagating from the sides of the structure which lowers the reflected overpressure.

I. INTRODUCTION

A. Background

During one of the meetings of the Blast Technology Subcommittee for the Revision of the Protective Structures Manual[1] it was pointed out that there was a data gap with regard to the effect of angle of incidence on reflected impulse impinging on finite structures. The effect of angle of incidence of the shock wave striking an infinite plane on peak reflected pressure and reflected impulse has been documented in many height of burst studies. The latest of these was conducted in Canada and reported in References 2 and 3. After a literature survey there appeared to be little information on the effect of angle of incidence on reflected impulse loading of isolated structures.

B. Objective

The objective of this study is to determine experimentally the effect of angle of incidence of the shock front on the reflected impulse loading on an isolated structure. The experiment was conducted with 1/50 scaled non-responding models of a single structure.

II. TEST PROCEDURES

This section will describe the procedure followed in conducting an experimental program to meet the stated objective.

A. Design of Model

The model was designed to represent a structure 15.24 metres wide by 15.24 metres long by 22.86 metres high (50 ft x 50 ft x 75 ft). A 1/50th scale produced a model 0.305 m x 0.305 m x 0.457 m (1 ft x 1 ft x 1.5 ft). The model was constructed of a 2.54 cm thick steel plate. A sketch of the model is presented in Figure 1. The four upright walls were welded together with the top bolted on to allow access to the pressure gages. A reinforced concrete mount with an anchor bolt imbeded (as shown in Figure 2) was used to secure the model. The pressure transducers were then installed and the top plate was bolted in place. An exploded view of the model, mount, and pressure transducers is shown in Figure 3. The model was held in place by tightening the large nut down against top plate. By loosening the nut, the model

---

[1] *Department of the Army, the Navy, and the Air Force, "Structures to Resist the Effects of Accidental Explosions," June 1969, TM5-1300, NAVFAC P-397, AFM 88-22.*

[2] *R.E. Reisler, B. Pettit and L. Kennedy, "Air Blast Data from Height of Burst Studies in Canada, Vol I: HOB 5.4 to 71.9 Feet," BRL Report No. 1950, December 1976 (AD#B016344L).*

[3] *R.E. Reisler, B. Pettit and L. Kennedy, "Air Blast Data from Height of Burst Studies in Canada, Vol. II, HOB 4.5 to 144.5 Feet," BRL Report No. 1990, May 1977.*

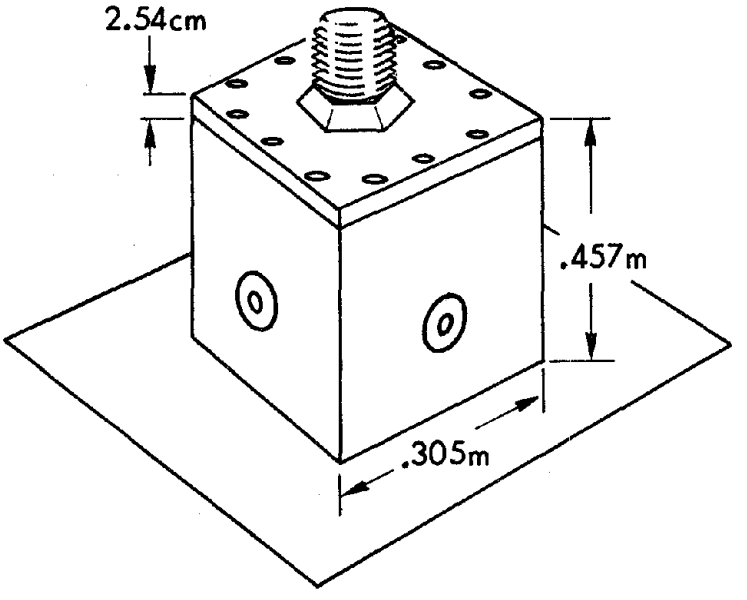

Figure 1. The 1/50th Scale Steel Structure Model.

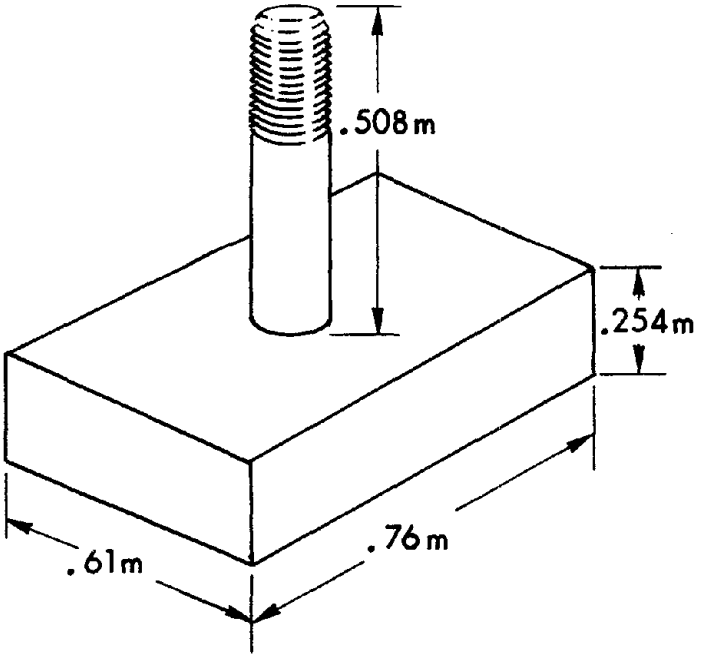

Figure 2. Concrete Mount with Anchor Bolt.

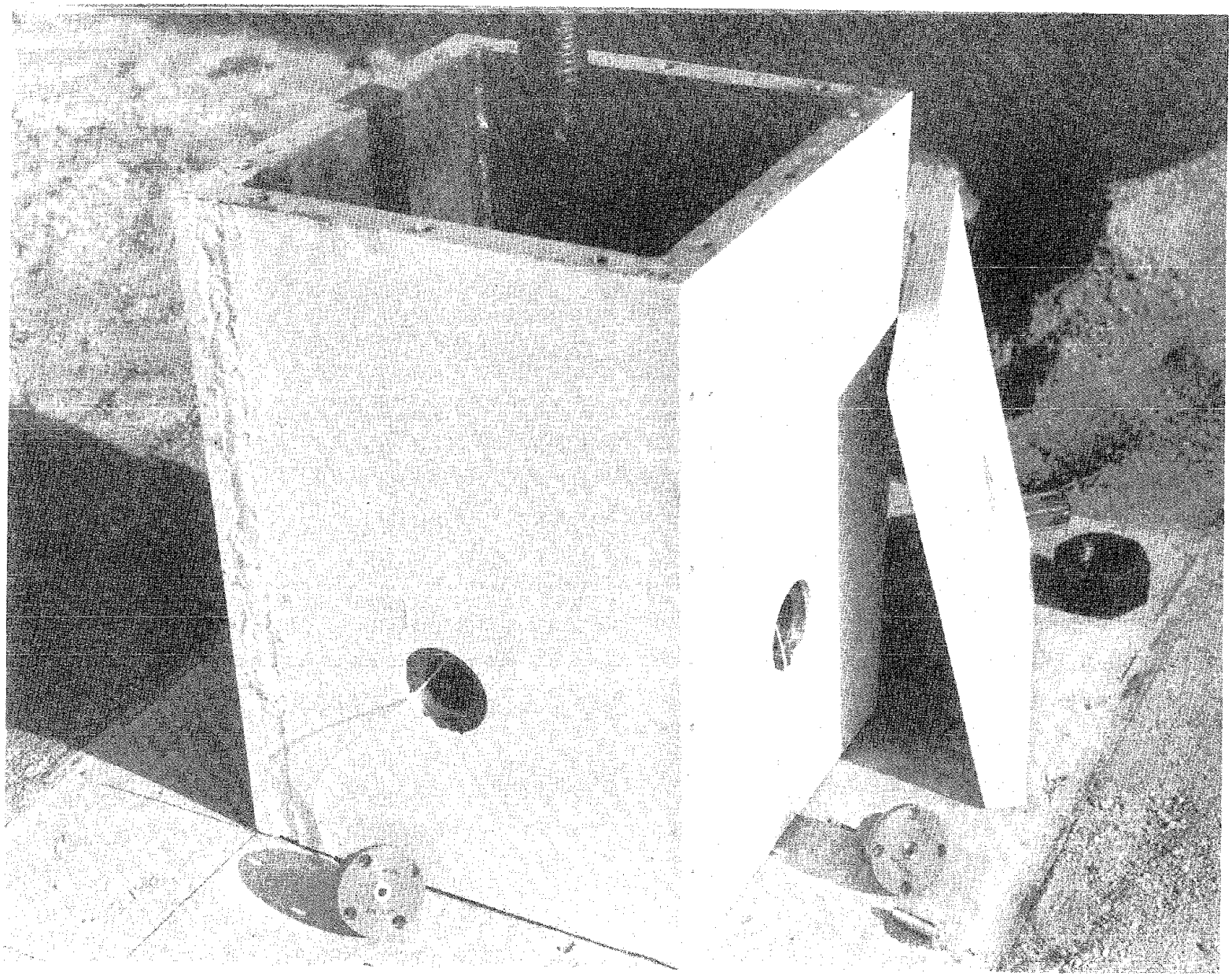

Figure 3. Exploded View of the Model, Mount, and Pressure Transducers.

orientation could be changed for each test and then retightened. A total of eight models was constructed. The pressure transducers were placed on the center line of a front and side wall at a height of 0.152 m. The model was rotated to change the angle of incidence of the shock front with the model walls.

B. Test Charges

The test charges were cast Pentolite (50 PETN, 50 TNT). The shape was hemispherical and the point of detonation was at the center of the flat side which was placed on the ground surface. The full size charge yield selected for simulation was 125000 kilograms. Therefore a 1/50 scale model would require (according to cube root scaling) a one kilogram charge. One kilogram cast Pentolite charges were used on all of the fifteen tests conducted.

C. Test Instrumentation

The instrumentation for this test series consisted of pressure transducers, magnetic tape recorder/playback, and a data reduction system. A block diagram is shown in Figure 4.

1. Pressure Transducers. Piezo-electric pressure transducers were used for this series of tests. The PCB Electronics Inc., models 112A22, 113A24, and 113A28, with quartz sensing elements and built-in source followers were used extensively.

2. Tape Recorder System. The tape recorder consisted of three basic units, the power supply and voltage calibrator, the amplifiers, and the FM recorder. The FM tape recorder was a Honeywell 7600 having a frequency response of 80 kHz. Once the signal was recorded on the magnetic tape it was played back and recorded on a Honeywell Visicorder. This oscillograph has 5 kHz frequency response and the overpressure versus time recorded at the individual stations can be read directly from the playback records for preliminary data analysis.

3. Data Reduction System. For the final data output, the tape signals were processed through an analog-to-digital converter, to a digital recorder-reproducer, and then to a computer. The computer (TEKTRONIX 4051) was programmed to apply the calibration values and present the data in the proper units for analysis. From the computer, the data is put on a digital tape from which the final form can be plotted or tabulated. The digital tape can be also stored for future analysis.

D. Test Layout

The test layout was planned to acquire the maximum amount of data for each test conducted. A total of eight peak overpressure levels was selected and therefore eight models were constructed. Twenty-one angles of incidence were selected with eleven bunched between 37.5 and 62.5 degrees in order to document the transition between regular reflection and Mach reflection. The test layout is shown in Figure 5. The peak overpressure range of interest for this project was from 345 kPa down to 6.89 kPa. The distances selected to

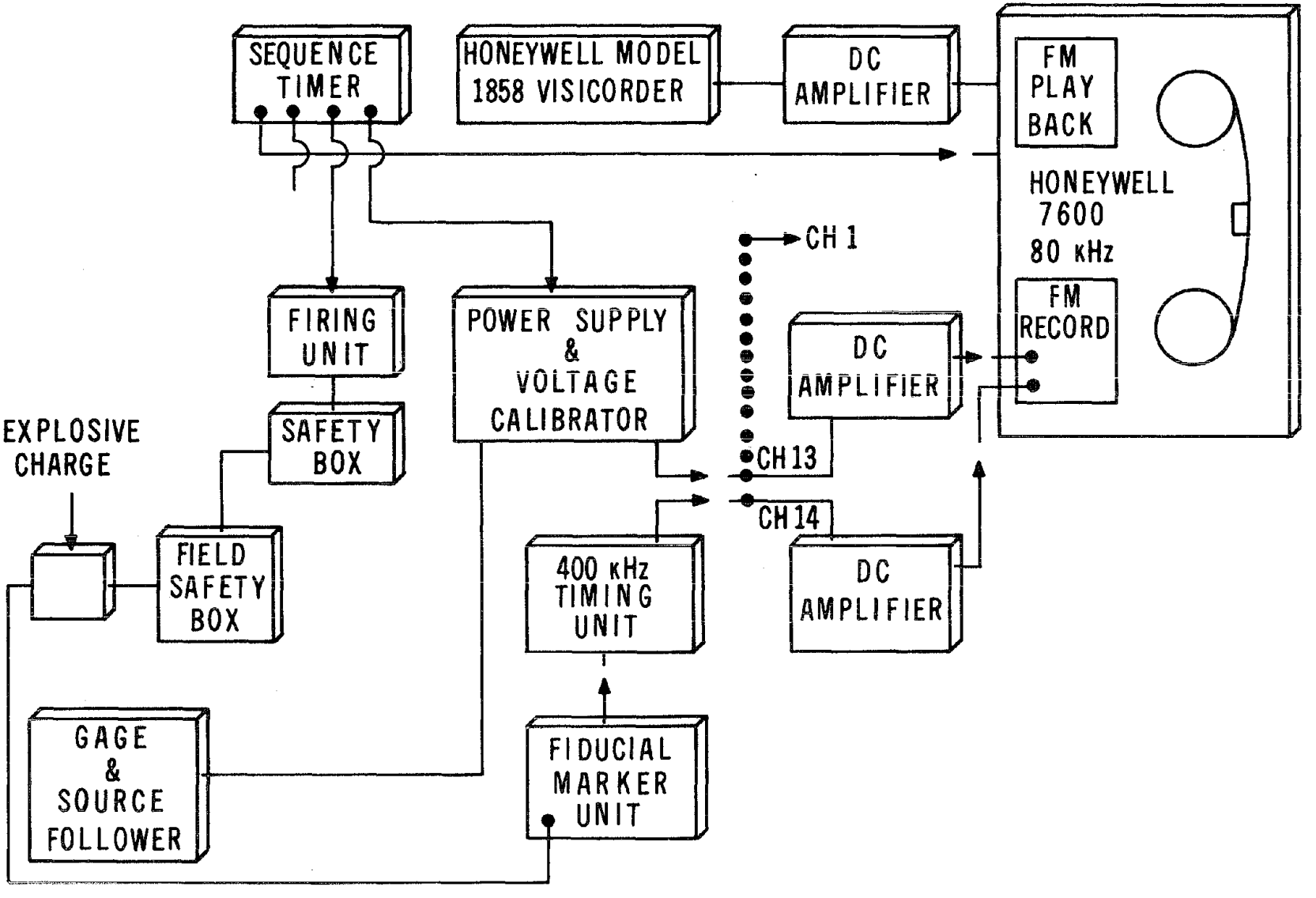

Figure 4. Instrumentation Block Diagram.

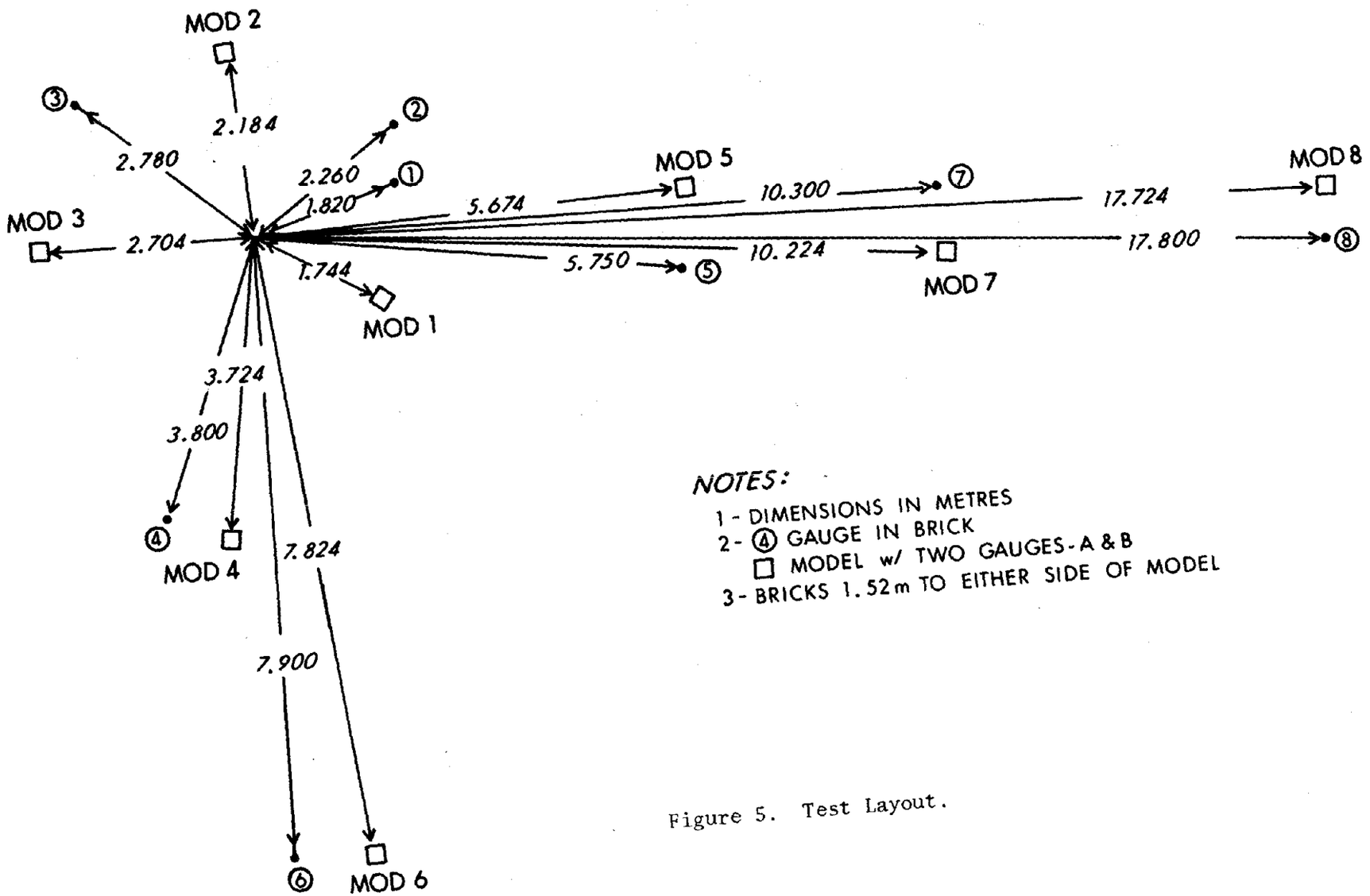

Figure 5. Test Layout.

meet the required pressure range were based on the standard TNT hemispherical surface burst curve.[4] The free-field incident peak overpressure was measured near each structure to provide the input blast parameters. Nomenclature used to identify the gage locations at each station is as follows: Station 1 is the free-field gage, Station 1A is in the front of the model wtih orientation from 0 to 45 degrees, and Station B is in the side of the model with orientation from 90 to 45 degrees. On Test 1, Station A on all models was at an angle of 0 degrees or normal reflection while Station B on all models was at an angle of 90 degrees or a side-on measurement. The station locations, predicted peak overpressures, and impulses are listed in Table 1 for Test Number 1. The locations of the free-field stations remained the same on all 15 tests. The radial distances for the Stations A and B changed on each shot. A photograph showing Structures 2 (foreground), 1, 4, and 6 for 0 degree and 90 degree orientation with a 1 kg charge in place is presented in Figure 6.

E. Test Matrix

Eight model structures were placed at the distances shown in Table 1 to receive the predicted input pressure and impulse. After each test, each model was rotated the same number of degrees in order that the shock front would strike each set of structure walls at the same angles of incidence. The angle of incidence for each test (1-12) is listed in Table 2. On Tests 13, 14, and 15 the structure models were exposed at different angles and at different pressure levels. These exposures are listed in Table 3.

F. Predictive Approach

There are many references in which the enhancement of peak overpressure as a function of angle of incidence is reported. One of the more complete treatments is given in Reference 5. Normal reflection or head-on reflection can be predicted for the range of incident overpressures of interest in these tests using the following equation:

$$P_r = 2\,P_s \left(\frac{7\,P_0 + 4\,P_s}{7\,P_0 + P_s} \right) \qquad (1)$$

where P_o = Ambient atmospheric pressure,
P_r = Normal reflected overpressure, and
P_s = Side-on incident overpressure.

This is valid where the ratio of specific heat (γ) for air is a constant 1.4. The equation is good only for predicting the reflected pressure when the models are in the 0-degree orientation, face-on.

---

[4] *C.N. Kingery, "Air Blast Parameters versus Distance for Hemispherical Surface Bursts," BRL Report 1344, September 1966 (AD#811673).*

[5] *"Nuclear Weapons Blast Phenomena, Volume II, Blast Wave Interaction," DASA 1200-II, 1 December 1970 (Confidential RD).*

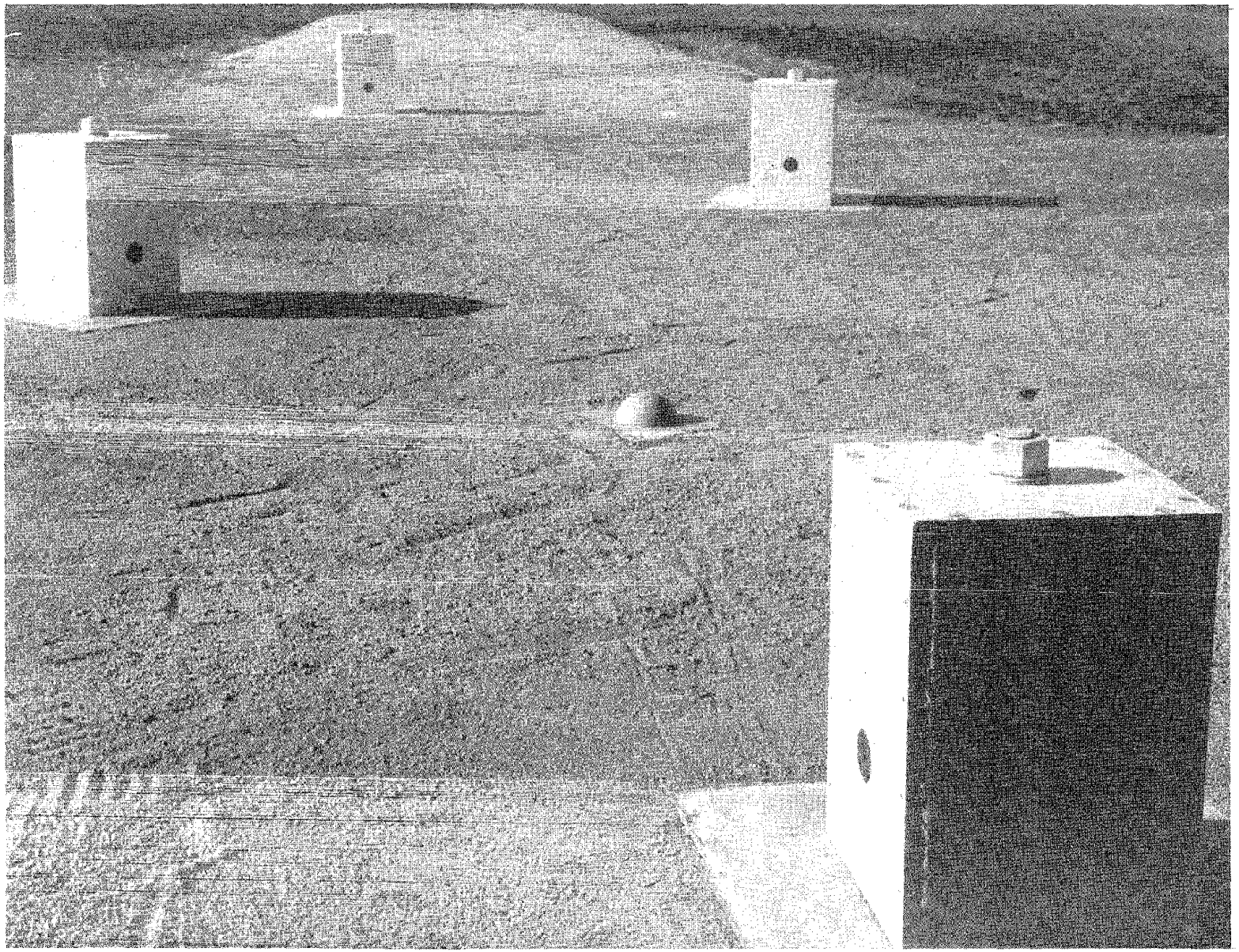

Figure 6. Photograph of Models 2, 1, 4, and 6 with 0 and 90 Degree Orientation.

TABLE 1. PREDICTED PEAK PRESSURES AND IMPULSES FOR TEST 1

Station	Distance m	Pressure kPa	Impulse kPa-ms	Station	Distance m	Pressure kPa	Impulse kPa-ms
1	1.82	345	145	5	5.75	34.5	51
1A	1.74	1361	430	5A	5.67	78.7	110
1B	1.90	340	140	5B	5.83	33.9	50
2	2.26	207	120	6	7.90	20.7	39
2A	2.18	695	320	6A	7.82	44.9	80
2B	2.34	190	112	6B	7.98	20.8	38
3	2.78	138	98	7	10.30	13.8	30
3A	2.70	408	250	7A	10.22	29.1	59
3B	2.86	130	96	7B	10.38	13.7	30
4	3.80	68.9	74	8	17.80	6.89	18
4A	3.72	164	170	8A	17.72	14.7	32
4B	3.88	66.0	72	8B	17.88	6.89	18

TABLE 2. MODEL ORIENTATION, TESTS 1-12

Test No.*	Angle of Incidence		Test No.	Angle of Incidence	
	A	B		A	B
1	0	90	7	37.5	52.5
2	10	80	8	40.5	49.5
3	16	74	9	42.5	47.5
4	21	69	10	43.5	46.5
5	27.5	62.5	11	45	45
6	34	56	12	0	90

*Tests 1 through 12 all models had same orientation

TABLE 3. MODEL ORIENTATION, TESTS 13-15

Station	1		2		3		4		5		6		7		8	
Test**	A	B	A	B	A	B	A	B	A	B	A	B	A	B	A	B
13	34	56	34	56	40.5	49.5	40.5	49.5	37.5	52.5	37.5	52.5	37.5	52.5	37.5	52.5
14	37.5	52.5	40.5	49.5	46.5	43.5	42.5	47.5	40.5	49.5	43.5	46.5	0	90	40.5	49.5
15	43.5	46.5	16	74	16	74	21	69	16	74	45	45	21	69	16	74

**On Tests 13, 14, and 15 models were oriented for repeat exposure at selected angles and pressure levels.

A second source used for predicting the reflected pressure in the regular reflection region for different angles of incidence is Reference 6. This report is based on a theoretical treatment by J. Von Newman. It considers the shock wave reflecting on an infinite plane as in a height of burst study. The reference does not treat impulse.

A newer source, Reference 7, treats both the enhancement of pressure in the regular reflection on rising slopes as well as the enhancement in the Mach reflection region on rising slopes. The reflected pressure versus incident pressure undergoing regular reflection for various rising slopes (Figure 12 from Reference 7) is presented as Figure 7. The reflected pressure versus incident pressure undergoing Mach reflection for various rising slopes (Figure 5 from Reference 7) is presented as Figure 8.

A family of curves from Reference 8 showing the reflection factor or pressure ratio P_r/P_s for selected input pressures (P_s) versus angle of incidence are presented in Figure 9. They were used in predicting the reflected pressure, P_r, expected to load the model. These curves and the other predictive methods will be compared with the field measurements.

III. RESULTS

As mentioned in the introduction, the primary objective of this project is to determine the enhancement of overpressure impulse as a function of the angle of incidence of the shock front striking an isolated structure. Presented in Section F of Test Procedures, are predictive approaches for determining the peak reflected pressure but there is a lack of information on predicting the reflected impulse other than normal or head-on. Information that is available, is from various height of burst studies, where the reflection process is on an infinite plane.

The results will be presented in the form of reflected pressure compared to side-on pressure or reflected pressure ratios (P_r/P_s). This comparison will also be done for impulse where ratios of I_r/I_s will be developed for angle of incidence and a variety of side-on or free-field impulses.

A. Side-on Overpressure and Impulse Measurements

In order to determine the pressure reflection and impulse reflection ratios, the side-on or incident overpressures and impulses must be established. Eight pressure transducers were placed at the distances and locations shown in Figure 5 to record the incident overpressure versus time of the blast wave. Records were obtained on each test and the incident peak

---

[6] *C.N. Kingery and B.F. Pannill, "Parametric Analysis of Regular Reflection of Air Blast," BRL Report 1249, June 1964 (AD#444997).*

[7] *Kenneth Kaplan, "Effects of Terrain on Blast Prediction Methods and Prediction," BRL Contract Report ARBRL-CR-00355, January 1978 (AD#A051350).*

[8] *Brode, H.L., "Height of Burst Effects at High Overpressures," The Rand Corporation, RM-6301, DASA 2506, July 1970.*

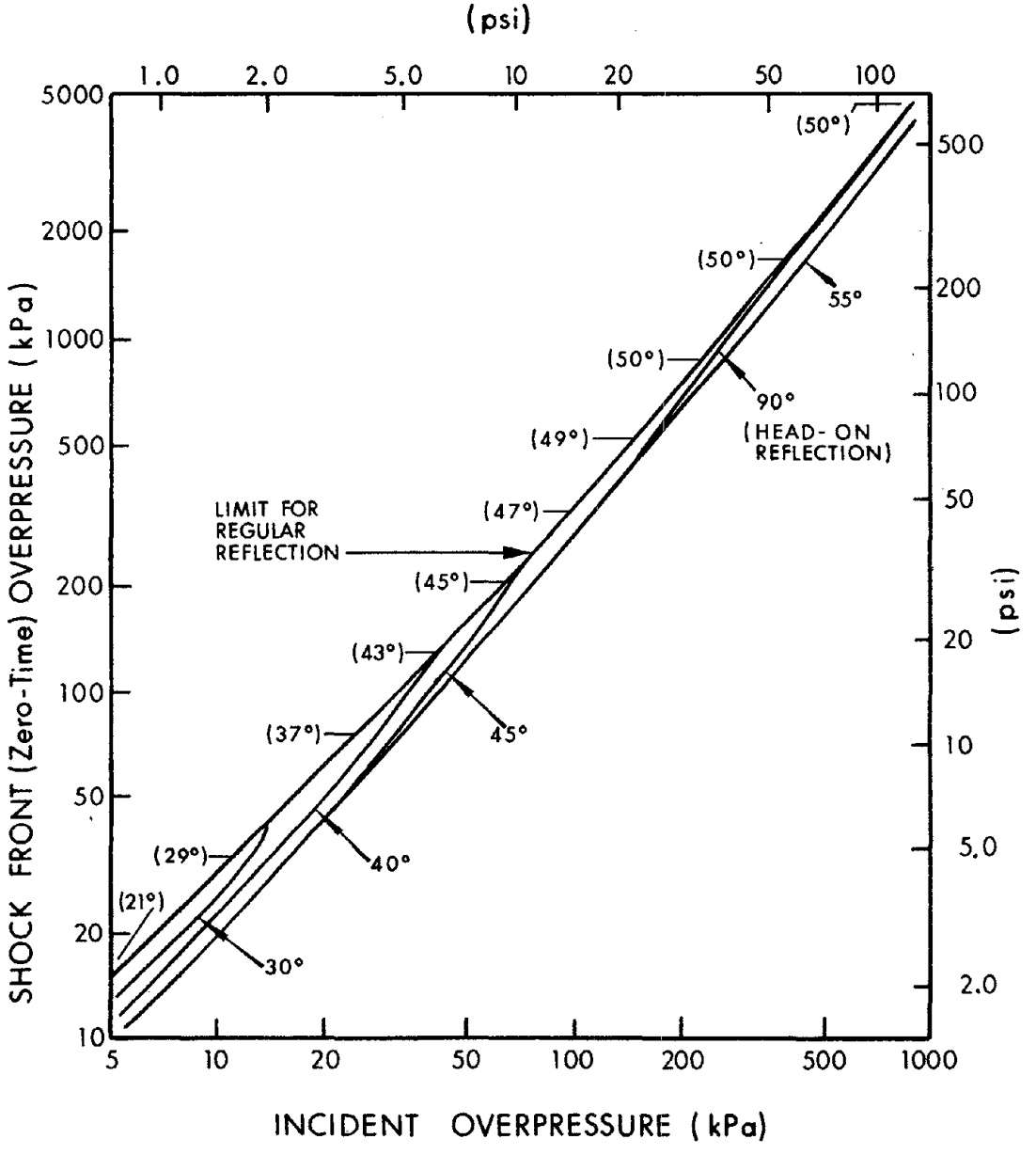

Figure 7. Reflected Pressure versus Incident Overpressure for a Shock Wave Undergoing Regular Reflection on a Rising Slope.

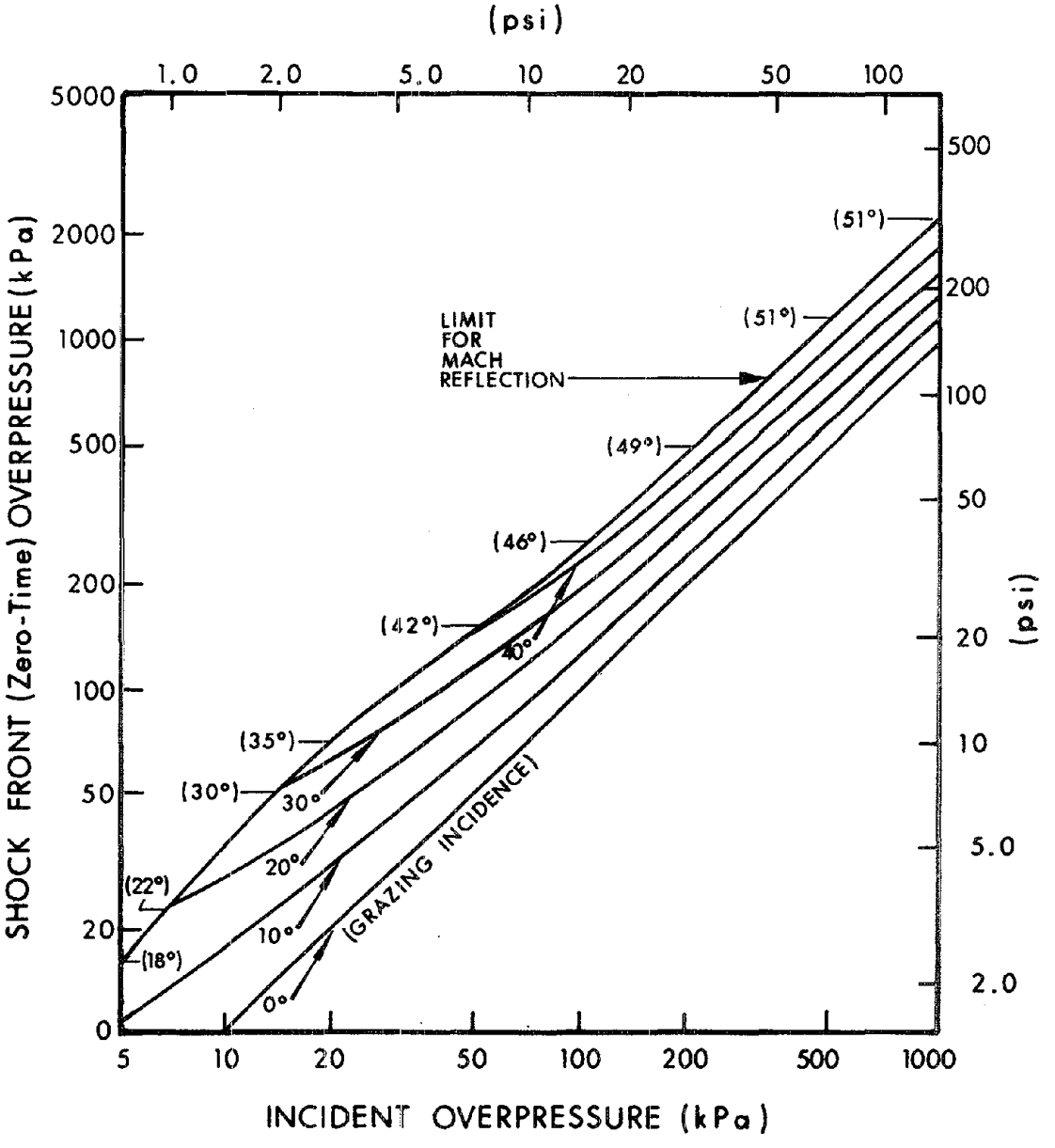

Figure 8. Reflected Pressure versus Incident Overpressure for Shock Waves Undergoing Mach Reflection on a Rising Slope.

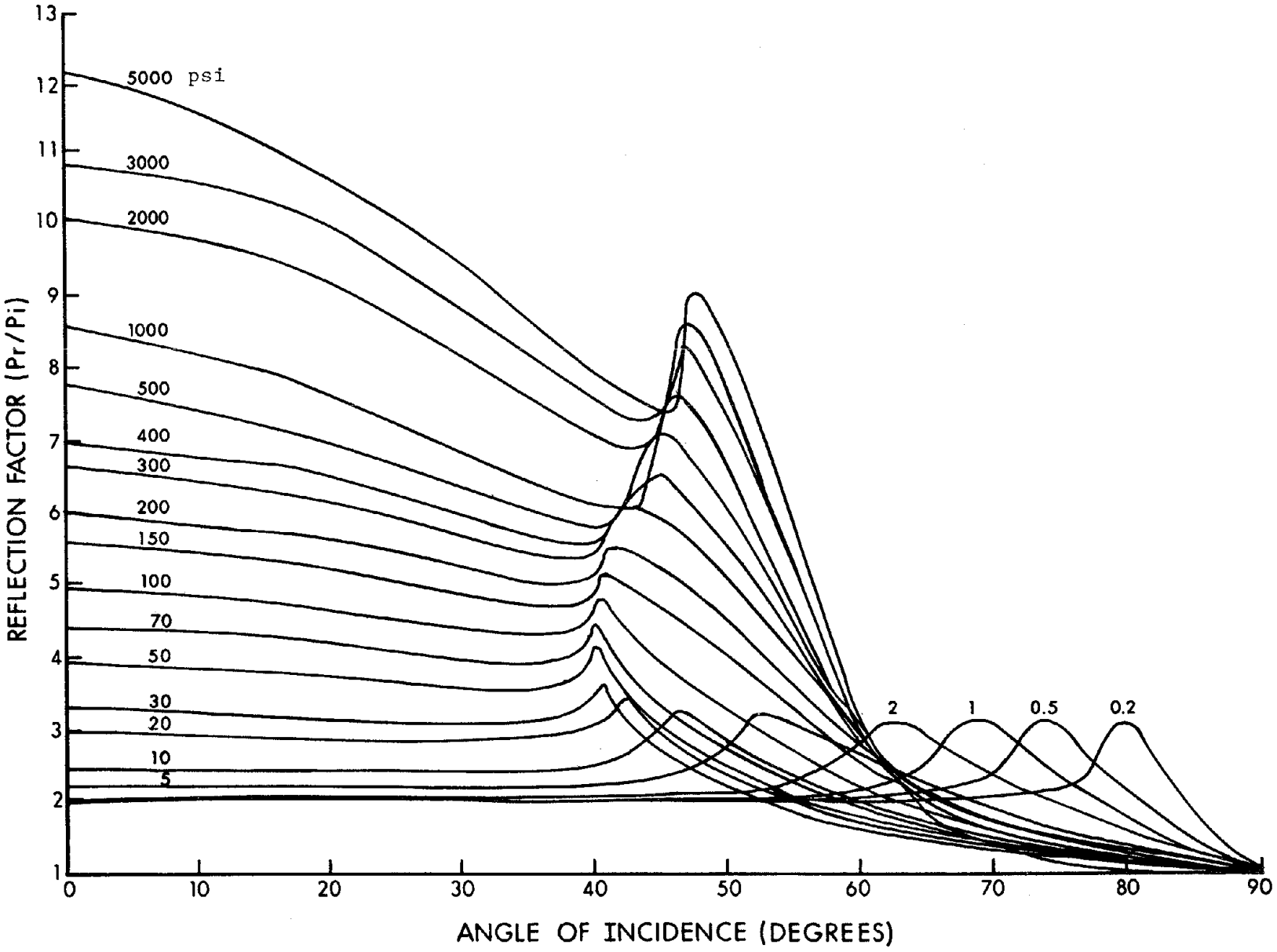

Figure 9. Reflection Factors versus Angle of Incidence for Selected Incident Overpressures.

overpressure and incident overpressure impulses are listed in Table 4 for each station. An average value from the fifteen tests was used to plot a peak overpressure versus distance for a 1 kg hemispherical Pentolite surface burst. Over ninety percent of the values of both pressure and impulse fell within a ± 5 percent of the average value established at each station. The average peak incident overpressure (P_s) versus horizontal distances are plotted in Figure 10. The solid lines in Figures 10 and 11 were established from data presented in Reference 9. The average incident impulses (I_s) versus horizontal distances from Table 4 are plotted in Figure 11.

B. Reflected Peak Overpressure and Impulse versus Angle of Incidence

The reflected peak overpressure versus angle of incidence is a direct measurement made on the front and side wall of the model. The reflected impulse is obtained from the integration of the overpressure versus time recorded from Stations A and B located on the model.

The reflected pressure recorded on Stations 1A and 1B through 8A and 8B are plotted versus angle of incidence in Figure 12. The lines through the data points are visual fits and were used to establish the values of reflected pressure listed in Table 5.

The reflected impulses versus angle of incidence recorded at Stations 1A and 1B through 8A and 8B are plotted in Figure 13. The solid lines are visual fits of the data points and were used to determine the values of reflected impulse listed in Table 5.

C. Reflected Pressure and Impulse Ratios versus Angle of Incidence

Both the reflected pressure (P_r) and the reflected impulse (I_r) will be presented as a function of side-on pressure (P_s) and side-on impulse (I_s) in the form of ratios. That is P_r/P_s and I_r/I_s will be presented versus angle of incidence.

The reflected pressure ratios P_r/P_s were calculated for each angle of incidence at each station and are listed in Table 5. It was noted in the Test Layout Section that Station A and Station B are located at different radial distances (ΔR) but this ΔR becomes less as the model is rotated and $\Delta R = 0$ at 45 degrees angle of incidence. In Table 5 the side-on pressure (P_s) for a θ of 0 degrees is listed for Station A and the P_s for 90 degrees is listed for Station B. The P_s for each radial distance from $\theta = 0$ degrees through $\theta = 90$ degrees was calculated to insure that the correct P_s for each angle was used in determining the ratio P_r/P_s. The values listed in Table 5 are plotted in Figures 14 and 15.

The reflected impulse ratios listed in Table 5 are based on the reflected impulse curves plotted in Figure 13 and the side-on impulse listed in Table 4 adjusted for the R distance between Station A and B. The range of side-on impulses is listed for each station in Table 5. The values of reflected impulse I_r divided by the side-on impulse I_s listed in Table 5 are plotted in Figure 16.

---

[9] *Charles Kingery and George Coulter, "TNT Equivalency of Pentolite Hemispheres," ARBRL-TR-02456, December 1982 (AD#A123340).*

TABLE 4. INCIDENT OVERPRESSURE AND IMPULSE AT FREE-FIELD STATIONS

Test No.	Station 1 Distance 1.82		Station 2 Distance 2.26		Station 3 Distance 2.78		Station 4 Distance 3.80	
	P_s kPa	I_s kPa-ms	P_s kPa	I_s kPa-ms	P_s kPa	I_s kPa-ms	P_s kPa	I_s kPa-ms
1	327	110	169*	103	121*	85	66	68
2	335	116	227	105	134	88	70	70
3	332	117	220	100	135	87	69	69
4	303	113	209	103	127	88	66	66
5	308	116	196	103	129	86	74	70
6	307	113	195	102	127	84	71	67
7	340	117	206	104	129	84	68	68
8	302	112	201	102	135	84	69	67
9	N-1	N-1	208	99	131	86	66	69
10	N-1	N-1	172*	106*	138	83	68	66
11	321	115	208	100	135	87	86*	286*
12	380*	116	190*	105	139	89	68	63*
13	315	121	215	99	139	85	71	67
14	324	114	206	108	131	91	72	69
15	292	120	212	104	140	91	69	71
AVG	317	115.4	208.6	102.6	133.5	86.5	69.1	68.2

*Questionable value
N-1 - Not instrumented

TABLE 4. INCIDENT OVERPRESSURE AND IMPULSE AT FREE-FIELD STATIONS (CONT)

Test No.	Station 5 Distance 5.75		Station 6 Distance 7.90		Station 7 Distance 10.3		Station 8 Distance 17.8	
	P_s kPa	I_s kPa-ms	P_s kPa	I_s kPa -ms	P_s kPa	I_s kPa-ms	P_s kPa	I_s kPa-ms
1	39	45	25	34	13.9	24.4	6.1	15.0
2	40	43	26	35	14.5	25.3	5.9	15.1
3	42	45	26	36	14.1	25.3	6.2	15.1
4	41	49	25	35	13.1	25.3	7.4	15.4
5	41	46	25	35	13.7	25.6	5.8	14.8
6	39	45	25	35	13.6	25.1	5.7	14.9
7	39	47	25	35	13.9	25.6	6.7	15.2
8	39	47	25	35	13.5	25.9	5.2	15.5
9	40	47	24	34	14.4	24.4	N-1	N-1
10	38	46	25	35	13.6	24.8	N-1	N-1
11	40	47	24	36	14.2	25.5	5.9	15.2
12	41	49	25	35	14.6	26.1	6.1	15.8
13	39	47	25	36	14.0	26.0	5.9	15.5
14	41	47	24	36	14.7	26.7	6.9	16.2
15	41	47	24	36	14.9	25.9	6.7	16.1
AVG	40.0	46.5	24.9	35.2	14.1	25.4	6.27	15.4

N-1 - Not instrumented

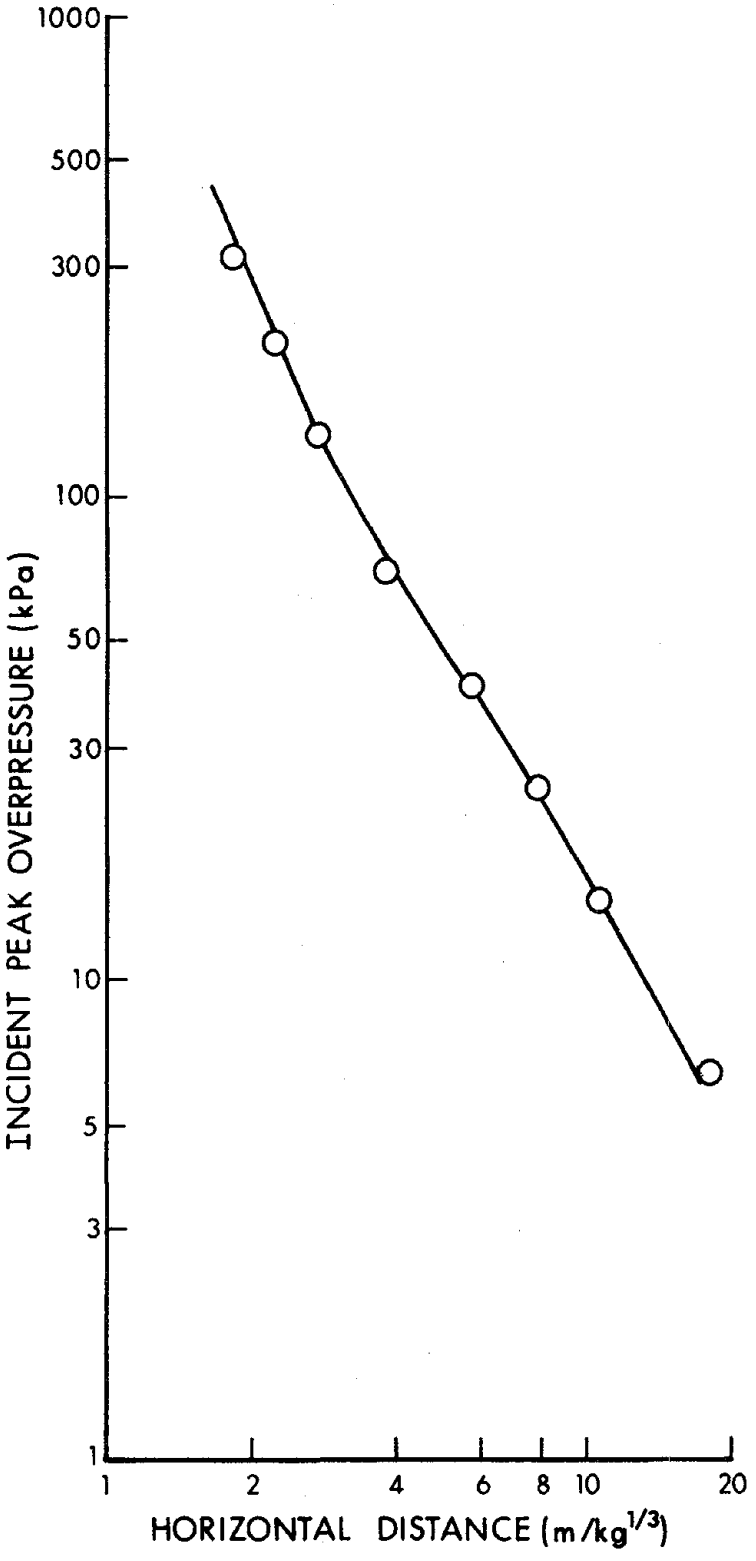

Figure 10. Peak Incident Overpressure versus Scaled Distance for a 1 kg Hemispherical Surface Burst.

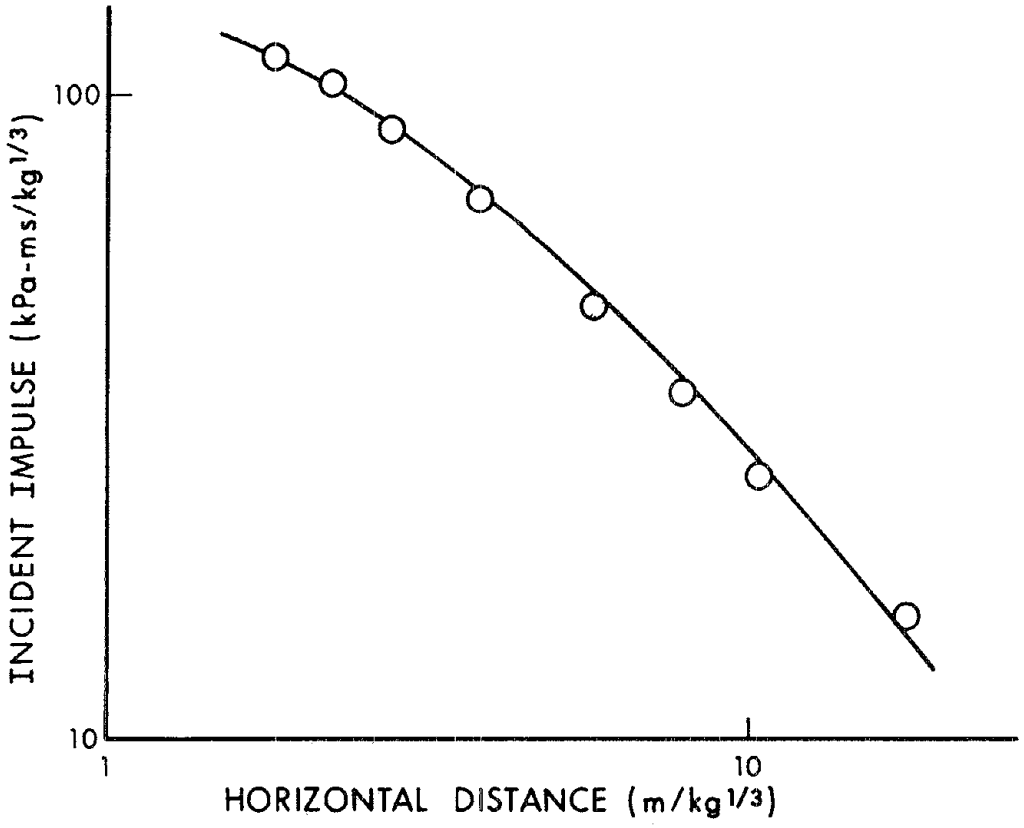

Figure 11. Incident Scaled Impulse versus Scaled Distance for a 1 kg Hemispherical Surface Burst.

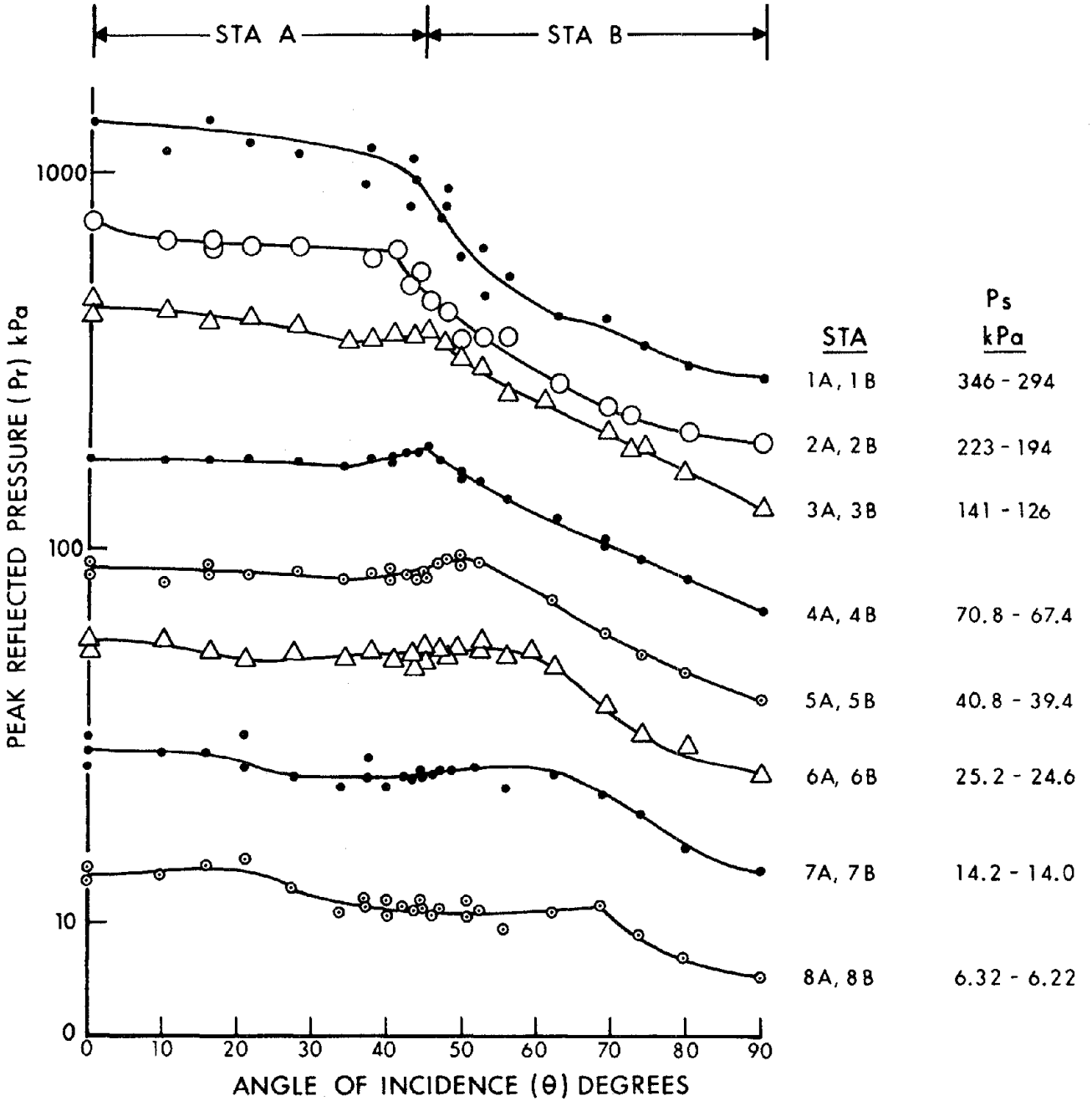

Figure 12. Peak Reflected Pressure versus Angle of Incidence for Stations 1 through 8.

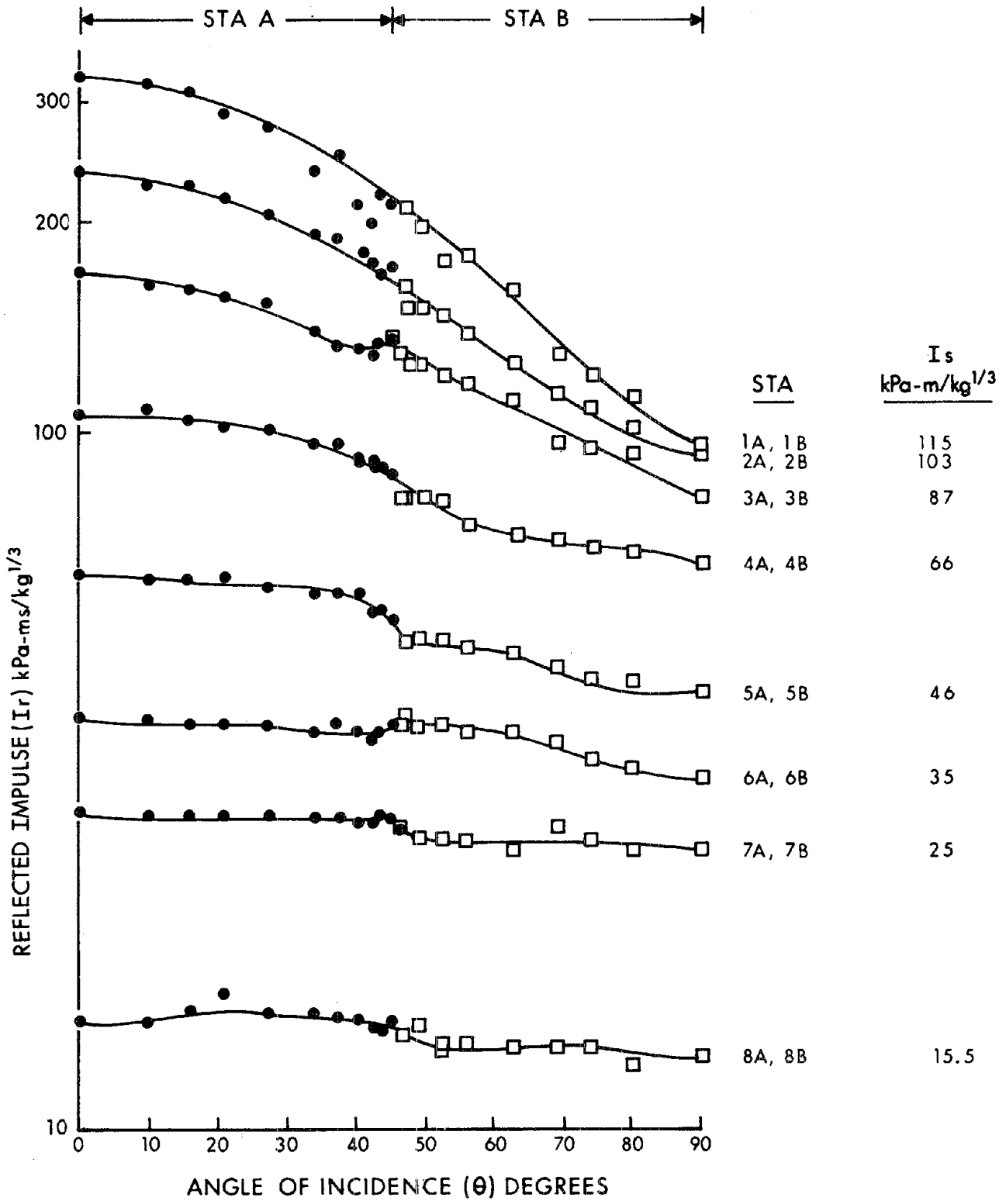

Figure 13. Scaled Reflected Impulse versus Angle of Incidence for Stations 1 through 8.

TABLE 5. REFLECTED PRESSURE AND IMPULSE RATIOS VERSUS ANGLE OF INCIDENCE

Station 1A, $P_s^* = 346$, $I_s^* = 118$					Station 1B, $P_s = 294$, $I_s = 113$				
Angle of Incidence degrees	REFL PRESS P_r kPa	PRESS REFL FACTOR P_r/P_s	REFL IMP I_r kPa-ms/kg$^{1/3}$	IMP REFL FACTOR I_r/I_s	Angle of Incidence degrees	REFL PRESS P_r kPa	PRESS REFL FACTOR P_r/P_s	REFL IMP I_r kPa-ms/kg$^{1/3}$	IMP REFL FACTOR I_r/I_s
0	1367	3.95	331	2.81	90	294	1.00	97	0.86
10	1310	3.81	325	2.75	80	310	1.06	114	1.01
16	1300	3.79	315	2.67	74	350	1.14	122	1.07
21	1280	3.74	291	2.47	69	390	1.25	130	1.14
27.5	1240	3.66	279	2.38	62.5	440	1.39	162	1.41
34	1200	3.57	237	2.03	56	500	1.56	180	1.55
37.5	1130	3.39	256	2.19	52.5	570	1.76	177	1.53
40.5	1050	3.16	213	1.82	49.5	650	1.99	200	1.72
42.5	950	2.88	201	1.72	47.5	750	2.29	211	1.82
43.5	900	2.73	221	1.89	46.5	812	2.48	212	1.83
45	850	2.58	215	1.85	45	850	2.58	215	1.85

*P_s unit - kPa

I_s unit = kPa-ms

TABLE 5. REFLECTED PRESSURE AND IMPULSE RATIOS VERSUS ANGLE OF INCIDENCE (CONT)

Station 2A, P_s = 223, I_s = 105					Station 2B, P_s = 194, I_s = 100				
Angle of Incidence degrees	REFL PRESS P_r kPa	PRESS REFL FACTOR P_r/P_s	REFL IMP I_r kPa-ms/kg$^{1/3}$	IMP REFL FACTOR I_r/I_s	Angle of Incidence degrees	REFL PRESS P_r kPa	PRESS REFL FACTOR P_r/P_s	REFL IMP I_r kPa-ms/kg$^{1/3}$	IMP REFL FACTOR I_r/I_s
0	760	3.41	240	2.29	90	194	1.00	94	0.94
10	690	3.09	232	2.21	80	205	1.03	104	1.03
16	650	2.93	230	2.19	74	224	1.11	110	1.09
21	650	2.94	220	2.10	69	240	1.18	116	1.14
27.5	650	2.95	210	2.02	62.5	277	1.34	129	1.26
34	640	2.94	195	1.88	56	325	1.55	140	1.36
37.5	620	2.86	192	1.85	52.5	370	1.75	149	1.45
40.5	510	2.59	183	1.76	49.5	410	1.93	152	1.48
42.5	520	2.42	175	1.68	47.5	430	2.02	151	1.47
43.5	520	2.33	170	1.65	46.5	460	2.16	164	1.59
45	480	2.25	173	1.68	45	480	2.25	173	1.68

TABLE 5. REFLECTED PRESSURE AND IMPULSE RATIOS VERSUS ANGLE OF INCIDENCE (CONT)

Station 3A, P_s = 141, I_s = 88					Station 3B, P_s = 126, I_s = 84				
Angle of Incidence degrees	REFL PRESS P_r kPa	PRESS REFL FACTOR P_r/P_s	REFL IMP I_r kPa-ms/kg$^{1/3}$	IMP REFL FACTOR I_r/I_s	Angle of Incidence degrees	REFL PRESS P_r kPa	PRESS REFL FACTOR P_r/P_s	REFL IMP I_r kPa-ms/kg$^{1/3}$	IMP REFL FACTOR I_r/I_s
0	433	3.07	172	1.95	90	126	1.00	81	0.96
10	431	3.06	165	1.88	80	160	1.25	94	1.11
16	420	2.98	163	1.85	74	184	1.40	96	1.13
21	405	2.89	159	1.81	69	206	1.57	97	1.13
27.5	390	2.81	155	1.76	62.5	235	1.77	112	1.30
34	360	2.61	140	1.59	56	275	2.05	118	1.36
37.5	365	2.64	134	1.52	52.5	305	2.26	123	1.41
40.5	380	2.77	134	1.54	49.5	330	2.43	127	1.46
42.5	380	2.77	131	1.51	47.5	348	2.56	127	1.46
43.5	385	2.81	136	1.56	46.5	362	2.66	131	1.51
45	390	2.87	138	1.59	45	390	2.87	138	1.59

TABLE 5. REFLECTED PRESSURE AND IMPULSE RATIOS VERSUS ANGLE OF INCIDENCE (CONT)

Station 4A, P_s = 70.8, I_s = 69					Station 4B, P_s = 67.4, I_s = 67				
Angle of Incidence degrees	REFL PRESS P_r kPa	PRESS REFL FACTOR P_r/P_s	REFL IMP I_r kPa-ms/kg$^{1/3}$	IMP REFL FACTOR I_r/I_s	Angle of Incidence degrees	REFL PRESS P_r kPa	PRESS REFL FACTOR P_r/P_s	REFL IMP I_r kPa-ms/kg$^{1/3}$	IMP REFL FACTOR I_r/I_s
0	177	2.50	107	1.55	90	69	1.02	64	0.96
10	175	2.48	109	1.58	80	84	1.25	67	1.00
16	178	2.52	106	1.54	74	92	1.35	68	1.00
21	178	2.52	103	1.49	69	103	1.50	70	1.03
27.5	172	2.44	101	1.46	62.5	122	1.77	72	1.06
34	161	2.38	96	1.39	56	138	1.99	74	1.07
37.5	176	2.52	97	1.41	52.5	157	2.26	82	1.21
40.5	178	2.55	92	1.33	49.5	164	2.36	82	1.19
42.5	183	2.61	91	1.32	47.5	172	2.47	80	1.16
43.5	183	2.61	90	1.30	46.5	173	2.48	81	1.17
45	189	2.71	89	1.29	45	189	2.71	89	1.29

TABLE 5. REFLECTED PRESSURE AND IMPULSE RATIOS VERSUS ANGLE OF INCIDENCE (CONT)

Station 5A, P_s = 40.8, I_s = 47					Station 5B, P_s = 39.4, I_s = 46				
Angle of Incidence degrees	REFL PRESS P_r kPa	PRESS REFL FACTOR P_r/P_s	REFL IMP I_r kPa-ms/kg$^{1/3}$	IMP REFL FACTOR I_r/I_s	Angle of Incidence degrees	REFL PRESS P_r kPa	PRESS REFL FACTOR P_r/P_s	REFL IMP I_r kPa-ms/kg$^{1/3}$	IMP REFL FACTOR I_r/I_s
0	93	2.28	63	1.34	90	40	1.02	42	0.91
10	89	2.18	62	1.32	80	48	1.21	44	0.96
16	88	2.16	62	1.32	74	52	1.31	44	0.96
21	87	2.14	62	1.32	69	60	1.50	41	1.00
27.5	88	2.16	60	1.28	62.5	73	1.83	48	1.04
34	84	2.07	59	1.25	56	83	2.06	49	1.04
37.5	85	2.10	59	1.25	52.5	91	2.26	50	1.06
40.5	87	2.15	59	1.25	49.5	94	2.34	50	1.06
42.5	86	2.13	55	1.17	47.5	93	2.31	49	1.04
43.5	85	2.10	56	1.19	46.5	91	2.25	50	1.06
45	88	2.18	54	1.15	45	88	2.18	54	1.15

TABLE 5. REFLECTED PRESSURE AND IMPULSE RATIOS VERSUS ANGLE OF INCIDENCE (CONT)

Station 6A, P_s = 25.2, I_s = 35					Station 6B, P_s = 24.6, I_s = 35				
Angle of Incidence degrees	REFL PRESS P_r kPa	PRESS REFL FACTOR P_r/P_s	REFL IMP I_r kPa-ms/kg$^{1/3}$	IMP REFL FACTOR I_r/I_s	Angle of Incidence degrees	REFL PRESS P_r kPa	PRESS REFL FACTOR P_r/P_s	REFL IMP I_r kPa-ms/kg$^{1/3}$	IMP REFL FACTOR I_r/I_s
0	56	2.22	39	1.11	90	25	1.02	32	0.91
10	56	2.22	39	1.11	80	29	1.17	33	0.94
16	52	2.06	38	1.09	74	32	1.30	34	0.97
21	50	1.98	38	1.09	69	38	1.53	36	1.03
27.5	52	2.07	38	1.09	62.5	48	1.93	37	1.06
34	51	2.03	37	1.06	56	52	2.09	37	1.06
37.5	52	2.07	38	1.09	52.5	54	2.17	38	1.09
40.5	50	2.00	37	1.06	49.5	53	2.12	38	1.09
42.5	50	2.00	36	1.03	47.5	51	2.04	39	1.11
43.5	50	2.00	36	1.03	46.5	52	2.08	38	1.09
45	52	2.08	38	1.09	45	52	2.08	38	1.09

TABLE 5. REFLECTED PRESSURE AND IMPULSE RATIOS VERSUS ANGLE OF INCIDENCE (CONT)

Station 7A, P_s = 14.2, I_s = 25					Station 7B, P_s = 14.0, I_s = 25				
Angle of Incidence degrees	REFL PRESS P_r kPa	PRESS REFL FACTOR P_r/P_s	REFL IMP I_r kPa-ms/kg$^{1/3}$	IMP REFL FACTOR I_r/I_s	Angle of Incidence degrees	REFL PRESS P_r kPa	PRESS REFL FACTOR P_r/P_s	REFL IMP I_r kPa-ms/kg$^{1/3}$	IMP REFL FACTOR I_r/I_s
0	30	2.11	28.7	1.15	90	14	1.00	25.0	1.00
10	29	2.04	28.0	1.12	80	16	1.14	25.0	1.00
16	29	2.04	28.0	1.12	74	20	1.43	26.0	1.04
21	29	2.04	28.0	1.12	69	22	1.57	27.0	1.08
27.5	26	1.83	28.0	1.12	62.5	25	1.79	25.0	1.00
34	25	1.77	28.0	1.12	56	26	1.84	26.0	1.04
37.5	26	1.84	28.0	1.12	52.5	26	1.84	26.0	1.04
40.5	25	1.77	27.5	1.10	49.5	26	1.84	26.0	1.04
42.5	25	1.77	27.5	1.10	47.5	26	1.84	26.0	1.04
43.5	25	1.77	28.0	1.12	46.5	25	1.80	27.0	1.08
45	25	1.80	28.0	1.12	45	25	1.80	28.0	1.12

TABLE 5. REFLECTED PRESSURE AND IMPULSE RATIOS VERSUS ANGLE OF INCIDENCE (CONT)

Station 8A, P_s = 6.32, I_s = 15.5					Station 8B, P_s = 6.22, I_s = 15.4				
Angle of Incidence degrees	REFL PRESS P_r kPa	PRESS REFL FACTOR P_r/P_s	REFL IMP I_r kPa-ms/kg$^{1/3}$	IMP REFL FACTOR I_r/I_s	Angle of Incidence degrees	REFL PRESS P_r kPa	PRESS REFL FACTOR P_r/P_s	REFL IMP I_r kPa-ms/kg$^{1/3}$	IMP REFL FACTOR I_r/I_s
0	13.2	2.09	14.2	0.92	90	7.2	1.16	12.6	0.82
10	13.5	2.14	14.2	0.92	80	8.2	1.31	12.2	0.79
16	14.0	2.21	14.8	0.95	74	9.9	1.58	13.2	0.86
21	14.0	2.21	15.6	1.01	69	11.0	1.76	13.1	0.85
27.5	12.4	1.97	14.6	0.94	62.5	10.9	1.74	13.1	0.85
34	11.2	1.77	14.5	0.94	56	10.5	1.67	13.1	0.85
37.5	11.3	1.79	14.5	0.94	52.5	10.9	1.74	13.0	0.84
40.5	11.3	1.79	14.4	0.93	49.5	11.0	1.75	14.0	0.91
42.5	11.1	1.76	13.9	0.90	47.5	11.0	1.75	13.5	0.88
43.5	10.8	1.72	13.8	0.89	46.5	11.0	1.75	13.5	0.88
45	11.4	1.81	14.3	0.93	45	11.4	1.81	14.3	0.93

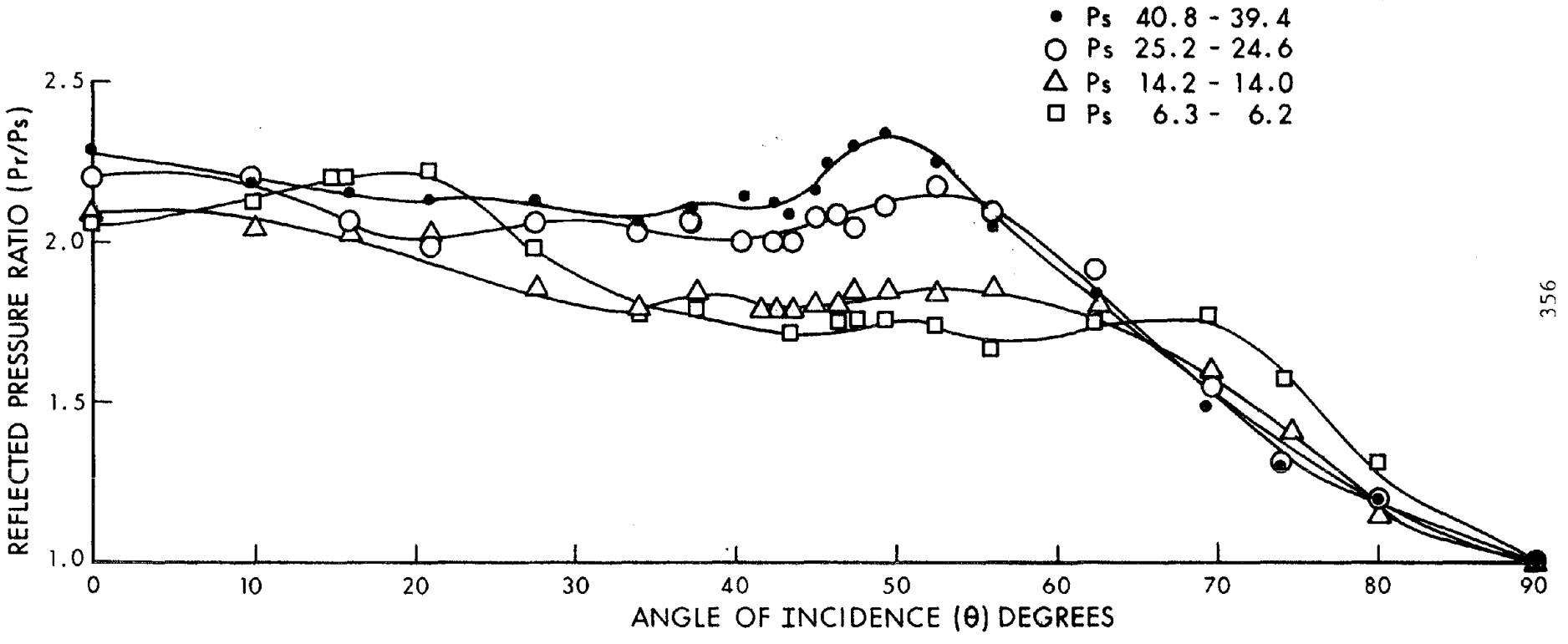

Figure 15. Reflected Pressure Ratios (P_r/P_s) versus Angle of Incidence for P_s from 40.8 kPa to 6.2 kPa.

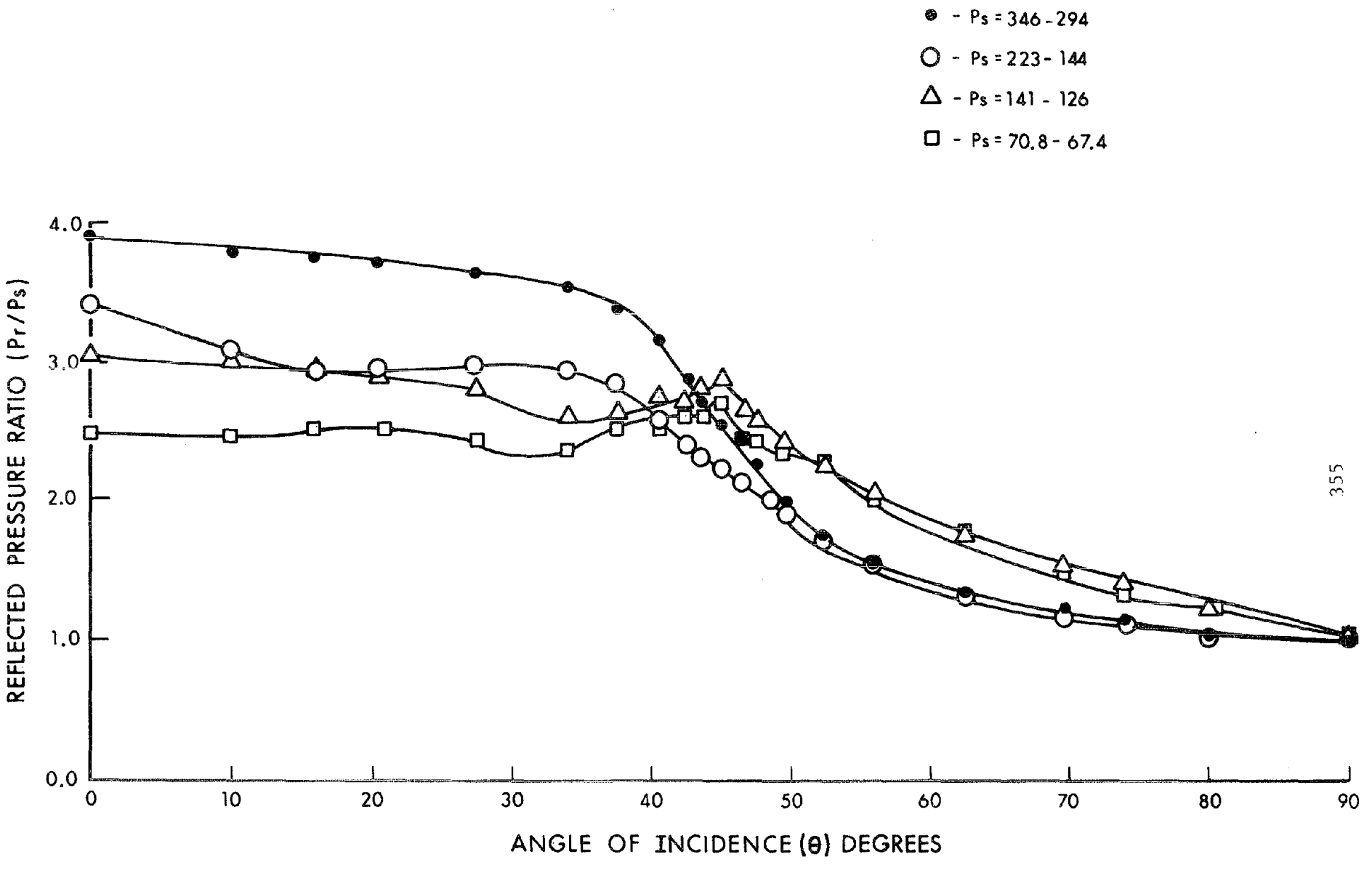

Figure 14. Reflected Pressure Ratios (P_r/P_s) versus Angle of Incidence for P_s from 346 kPa to 67.4 kPa.

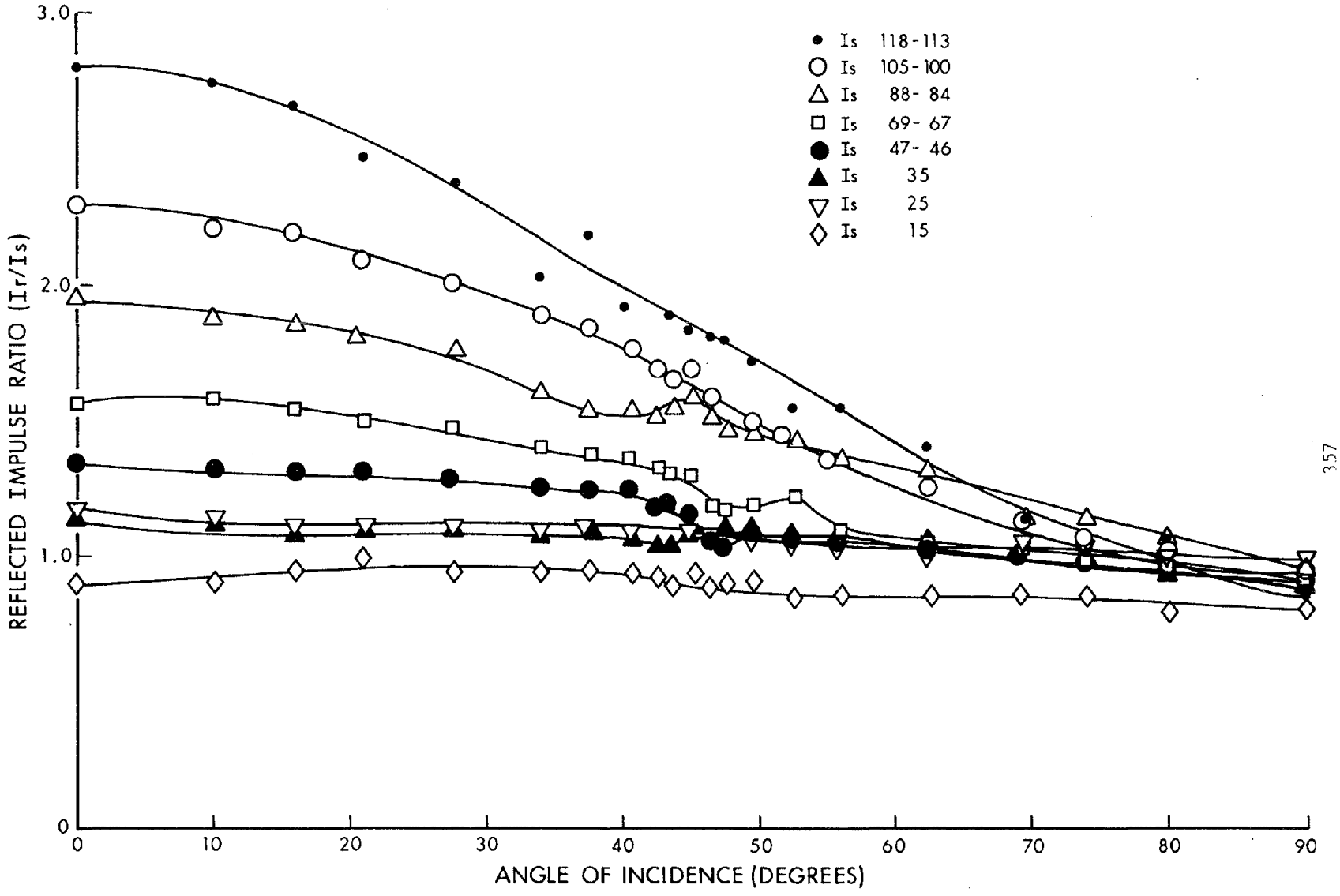

Figure 16. Reflected Impulse Ratios (I_r/I_s) versus Angle of Incidence.

IV. DISCUSSION

The data tables and plotted curves presented in the Results Section show trends of the effects on reflected pressure and impulse, of the angle of incidence of the shock front striking an isolated structure. Some of these trends follow theory and predictions as presented in the Predictive Approach of the Test Procedures Section while other results are different.

A. Reflected Pressure in the Regular and Mach Reflection Region

The curve showing reflective pressure (P_r) as a function of incident pressure (P_s) for all angles of incidence in the regular reflection region is shown in Figure 17. This curve is quite similar to the family of curves presented in Figure 7. Note in Figure 7 the slope angles are identified rather than the angle of incidence. The spread of data is indicated by the band at each station location. This means that when a particular station receives the same incident pressure (P_s) and as the model is rotated to change the angle of incidence the reflected pressure (P_r) does not change greatly in the regular reflection region. This is shown graphically in Figure 12.

The family of curves presented in Figure 18 show a trend similar to that presented in Figure 8, for pressure enhancement in the Mach reflection region. The quantitative values are higher in Figure 8, than measured experimentally in Figure 18. This difference is because the measured values from this series did not record the enhancement at the transition zone from the regular reflection region to the Mach reflection region as shown in Figure 9. The enhancement shown in Figure 9 is of very short duration and would have little effect on impulse in the blast wave.

B. Reflected Impulse in the Regular and Mach Reflection Regions

The reflected impulse versus incident impulse and angle of incidence is presented in Figure 13. A variation of this presentation is made in Figure 19 where the data is plotted for reflected impulse I_r, as a function of incident impulse (I_s) in the regular reflection region. The two solid lines show the variation in reflected impulse measured on an isolated structure when the angle of incidence is in the regular reflection region.

The dashed line presented in Figure 19 is to show the difference in the zero degree or head-on reflected impulse on an infinite plane and that recorded on a finite model. The lower values recorded on the model are because of the arrival of the rarefaction waves from the sides of the structure causes an increase in the rate of decay of the reflected pressure which produces a lower reflected impulse.

The reflected impulse recorded in the Mach reflection region is plotted in Figure 13 and presented in a different manner in Figure 20. In this figure the enhancement of reflected impulse becomes less as the angle of incidence approaches 90 degrees, or side-on conditions. The vortex from the front corner of the structure causes a lowering of the overpressure during the passage of the blast wave and the reflected impulse becomes less than the side-on impulse at an angle of incidence of 90 degrees. This is also true at some of the values measured at an 80 degree angle of incidence.

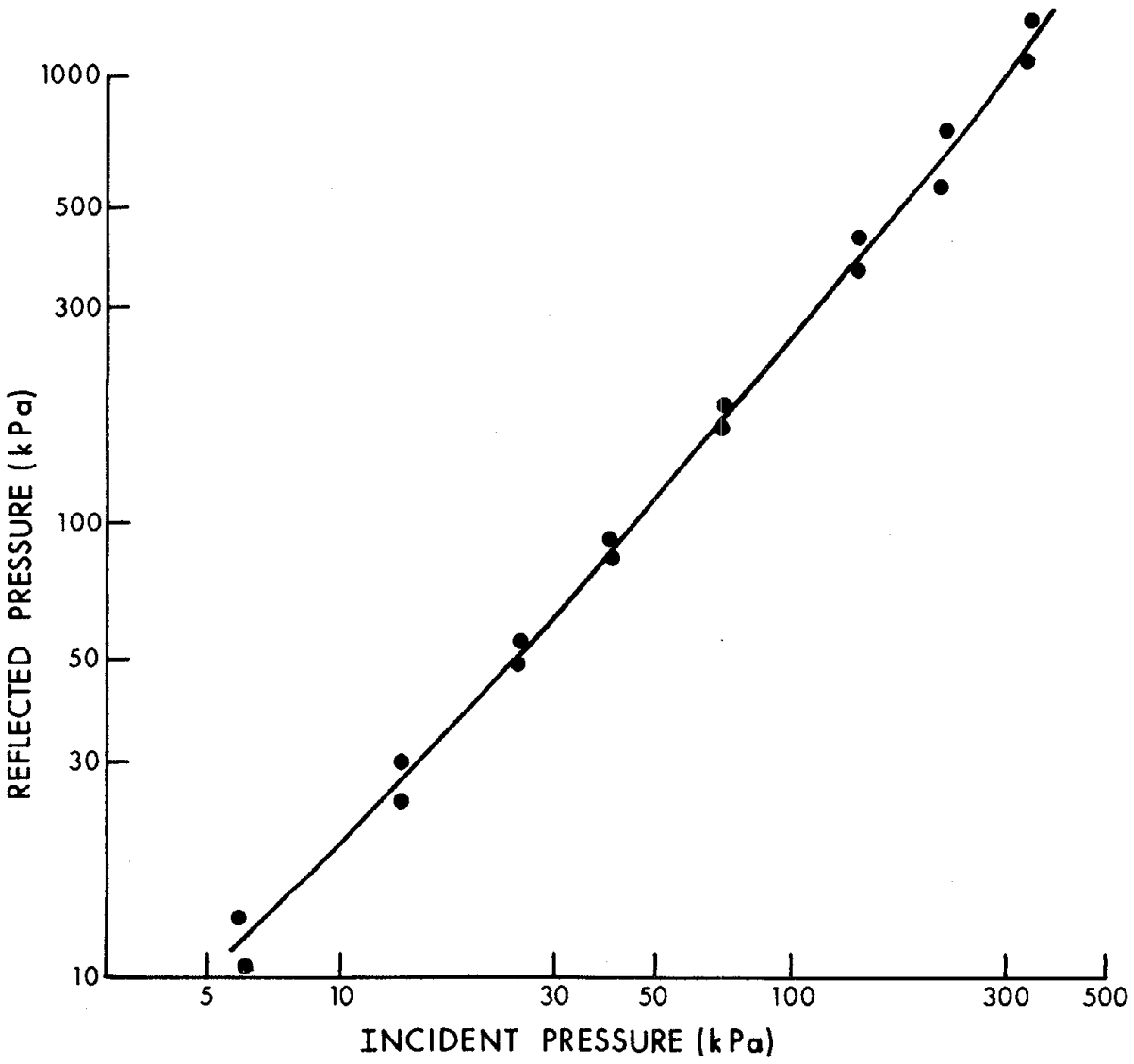

Figure 17. Reflected Pressure versus Incident Pressure in the Regular Reflection Region.

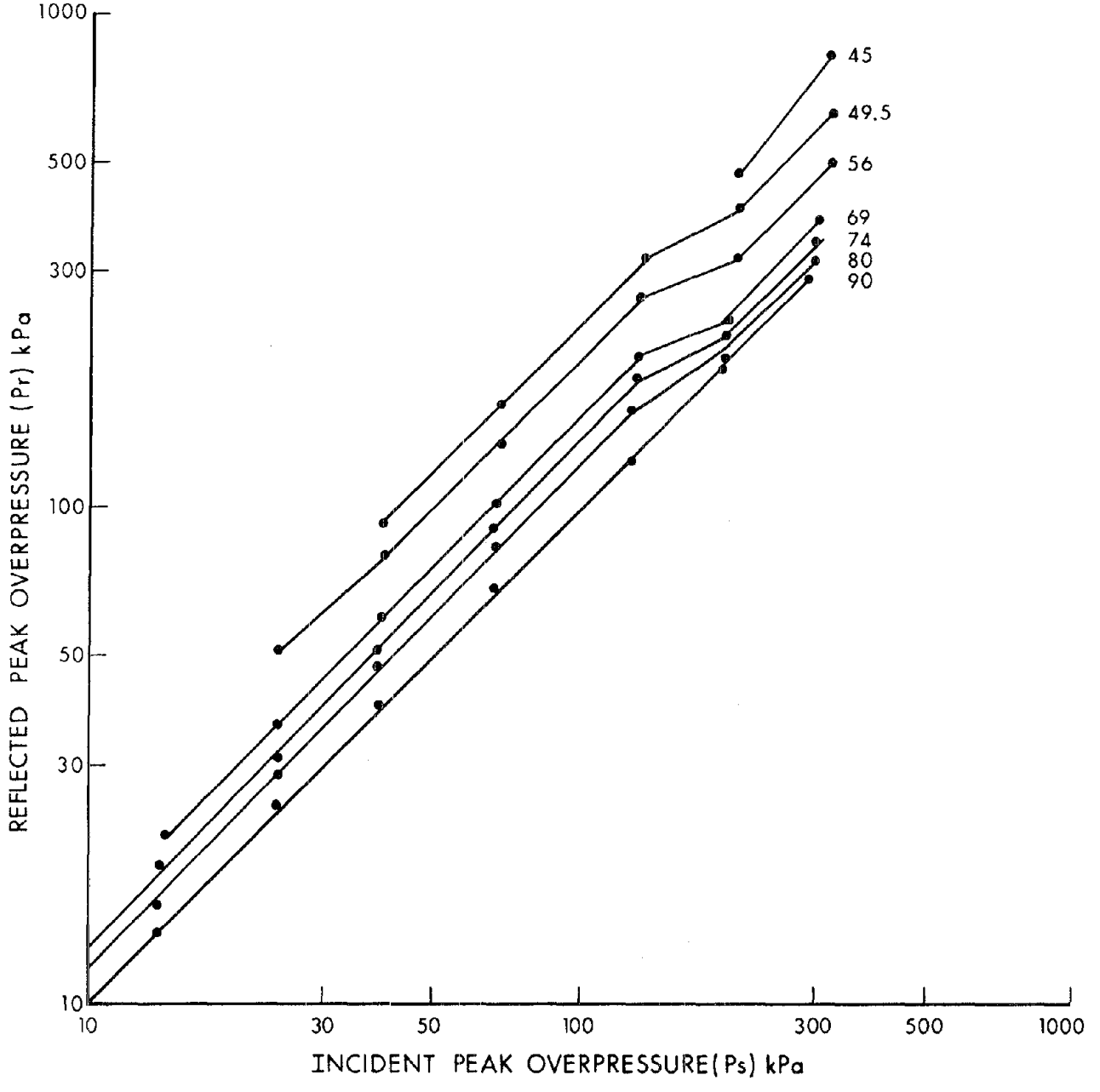

Figure 18. Reflected Pressure (P_r) versus Incident Pressure (P_s) in the Mach Reflection Region as a Function of Angle of Incidence.

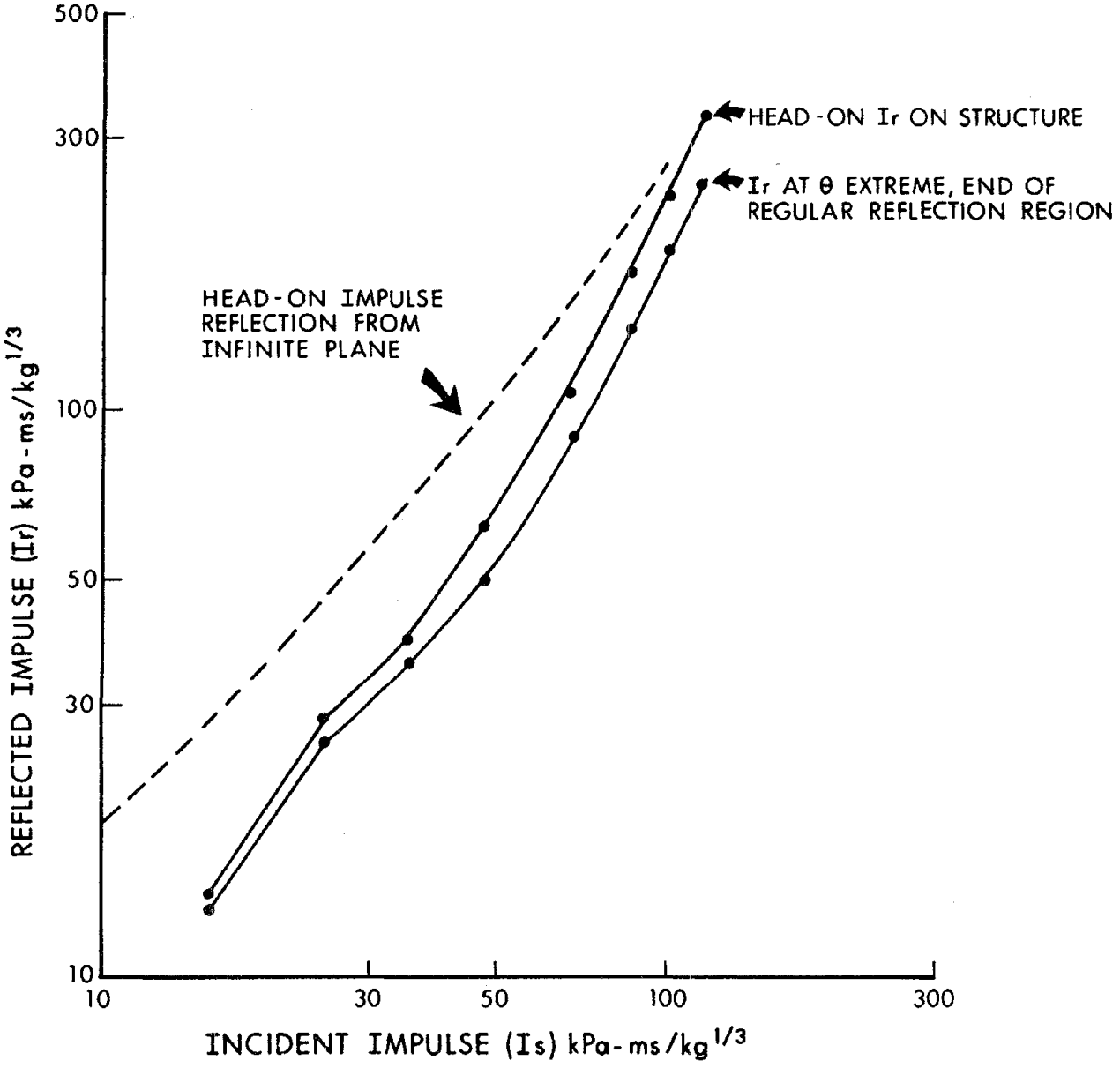

Figure 19. Scaled Reflected Impulse (I_r) versus Scaled Incident Impulse (I_s) in the Regular Reflection Region.

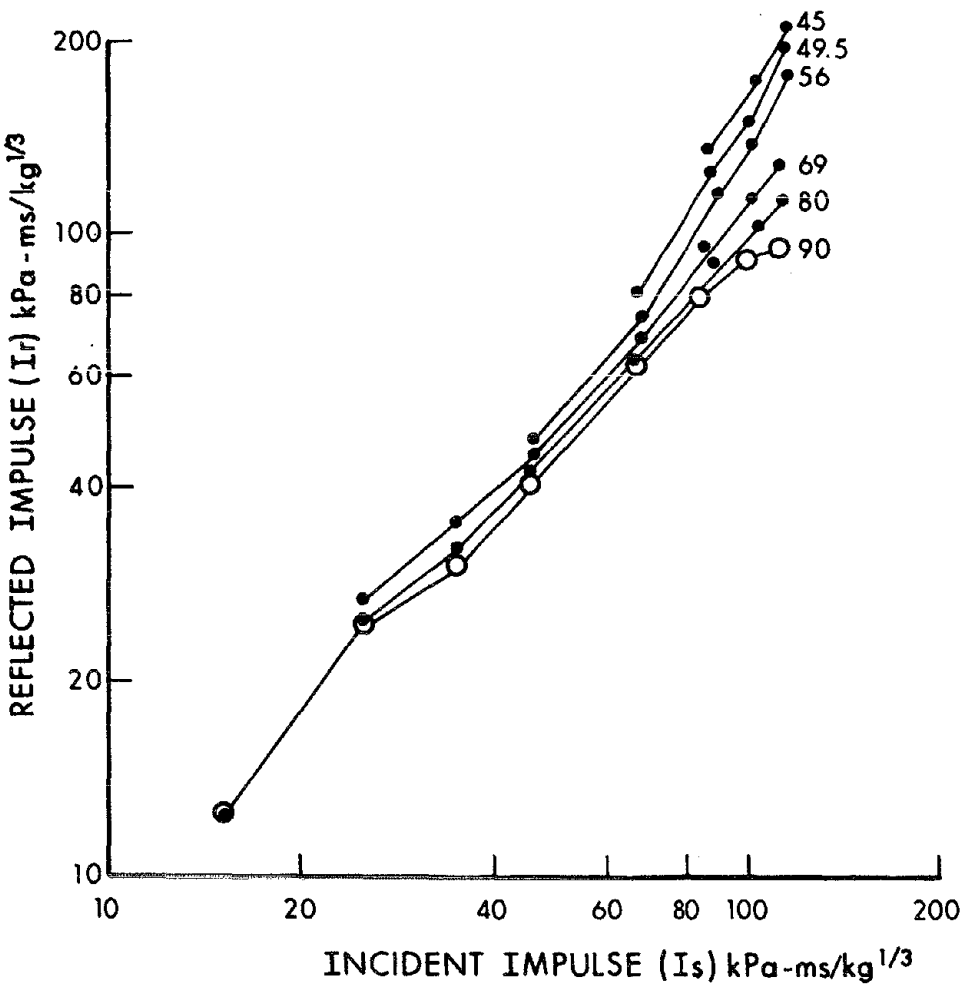

Figure 20. Scaled Reflected Impulse (I_r) versus Scaled Incident Impulse (I_s) in the Mach Reflection Region as a Function of Angle of Incidence.

V. CONCLUSIONS

The results presented in this report are based on one size structure and one charge mass. Therefore they cannot be applied in general to all size structures and all charge masses. The model was 0.3048m x 0.3048m x 0.4572m exposed to a 1 kg charge mass. This means the results could be applied to structures where the size is increased by the cube root of the charge mass. For example, a 1000 kg charge mass and a 3.048 metre structure or a 125000 kg charge and a 15.24 metre structure or a 512000 kg charge mass and a 24.38 metre structure 36.58 metres high. Care would have to be exercised in applying the results to other combinations of charge mass and structure dimensions. If a charge mass is held constant and the structure size increased, the reflected impulse values in the regular reflection region would approach the infinite plane case.

ACKNOWLEDGEMENTS

The authors wish to acknowledge the outstanding work of Mr. S. Dunbar, the electric engineer in charge of the instrumentation facility, who was responsible for recording all of the overpressure versus time data. He also processed the analog magnetic data tape through the data conversion computers to produce the information in digital form for plotting and analysis.

The authors also wish to acknowledge the work of Mr. K. Holbrook, technician and explosives handles for the excellent job done in site preparation, blast line installation, and model instrumentation and placement.

LIST OF REFERENCES

1. Department of the Army, Navy, and Air Force, "Structures to Resist the Effects of Accidental Explosions," June 1969, TM5-1300, NAVFAC P-397, AFM 88-22.

2. R.E. Reisler, B. Petit, and J. Kennedy, "Air Blast Data from Height of Burst Studies in Canada, Vol I: HOB 5.4 to 71.9 Feet," BRL Report No. 1950, December 1976 (AD#B016344L).

3. R.E. Reisler, and J. Kennedy, "Air Blast Data from Height of Burst Studies in Canada, Vol II: HOB 4.5 to 144.5 Feet," BRL Report No. 1990, May 1977.

4. C.N. Kingery, "Air Blast Parameters versus Distance for Hemispherical Surface Bursts," BRL Report 1344, September 1966 (AD# 811673) (AD#811673).

5. "Nuclear Weapons Blast Phenomena, Vol.II, Blast Wave Interaction," DASA 1200-II, December 1970 (Confidential RD).

6. C.N. Kingery and B.F. Pannell, "Parametric Analysis of Regular Reflection of Air Blast," BRL Report 1249, June 1964 (AD#444997).

7. Kenneth Kaplan, "Effects of Terrain on Blast Prediction Methods and Prediction," BRL Contract Report ARBRL-CR-00355, January 1978 (AD#A051350).

8. H.L. Brode, "Height of Burst Effects at High Overpressure," The Rand Company, RM-6301, DASA 2506, July 1970.

9. Charles Kingery and George Coulter, "TNT Equivalency of Pentolite Hemispheres," ARBRL-TR-02456, December 1982 (AD#A123340).

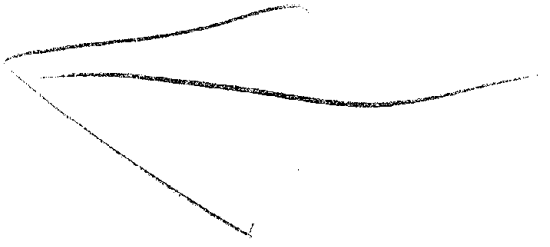

Chemical Demilitarization: Disposing of the Most Hazardous Wastes

John A. Scott
and
Richard Rife

US Army Toxic and Hazardous Materials Agency
Aberdeen Proving Ground, MD 21010

This country's aging stockpile of chemical warfare (CW) munitions will eventually require safe and economical disposal. These CW munitions present a unique challenge for demilitarization, since handling of both explosives and toxic material is required. The first full scale projectile disposal facility is presently under design; construction will start on Johnston Island in the summer of 1985. The technology developed for incorporation into the Johnston Atoll Chemical Agent Disposal System (JACADS) maximizes the use of automated equipment, provides the containment necessary to protect the worker and environment, and thermally destroys both the toxic fill and explosives from the CW munitions.

For several decades the United States manufactured CW munitions. Although manufacturing was halted in the late 1960's, large quantities of CW items remain stored in ammunition magazines at eight US Army installations. Periodic inspections performed by ammunition surveillance personnel to verify the condition of these stored items result in munitions being placed into one of several condition codes. Whenever a munition lot is determined to be unserviceable/unrepairable, or becomes obsolete, it is placed into "Condition Code H", to await disposal. At this point it becomes some of this country's most hazardous waste.

Munition types which make up this country's CW stockpile include bombs, rockets, land mines, spray tanks, cartridges, mortars, projectiles, and bulk containers. Disposal of these CW munitions presents a unique challenge, since these items may contain both energetic materials (explosive components) and an extremely toxic fill (chemical agent). (Not all CW munitions are explosively configured; many munitions are stored separately from the explosive components.) The special hazards associated with chemical demilitarization operations require considerable safeguards in order to dispose of this material in a safe and environmentally acceptable manner.

In response to these requirements, the Army has developed methods and procedures on the leading edge of technology for hazardous waste disposal.

This country's CW stockpile is 16-30 years old. The agent contained within the munitions is even older. Although chemical stabilizers were added during agent manufacture, deterioration of the agent fill has occurred during prolonged storage. A special study commissioned by the Department of Defense found that the munition components were not experiencing any metallurgical degradation; however, the study concluded that

the agent was expected to continue to deteriorate. The study predicted 50% ± 10% of the agent would remain in 1990. Another finding was the possibility of catastrophic agent decomposition, once the stabilizer is depleted.[1] These considerations, coupled with this country's efforts to achieve a verifiable ban on chemical weapons, are driving the need for planning for construction of appropriate disposal facilities.

CW munitions presently in storage were not designed to facilitate their eventual disposal; early disposal of CW materiel was primarily accomplished by burial at sea, the last at sea burial being Operation Chase X, in August 1970. Rising worldwide environmental concern led the Department of Army (DA) to commission a study by the National Academy of Sciences (NAS) to investigate disposal alternatives for CW munitions. In response, the NAS concluded "...that all such agents and munitions will require eventual disposal and that dumping at sea should be avoided. Therefore, a systematic study of optimal methods of disposal on appropriate military installations, involving no hazards to the general population and no pollution of the environment, should be undertaken. Appropriately, large disposal facilities should be a required counterpart to existing stocks and planned manufacturing operations. As the first step in this direction, we suggest the construction of facilities for gradual demilitarization and detoxification...".[2] The NAS recommendations for chemical demilitarization were supplemented by DA guidance to insure absolute safety and security rather than cost or time, maximum protection for operating personnel, absolute assurance of total containment of agent, and collection of incontrovertible data to justify personnel safety, security, and community safeguard.

Chemical munitions are maintained in storage in a variety of configurations: some include fuzes, explosive burster charges, and propellant. Lethal chemical agents currently available for military application include mustard and nerve agents. Table 1 illustrates the various munitions which the disposal process must handle and Table 2 provides data on the toxic agents.

Chemical warfare agents are extremely toxic compounds that produce lethal or incapacitating effects on man, depending upon the degree of exposure. (Excluded are riot control agents, chemical herbicides, and smoke and flame materials.)

The term nerve agents refers to two groups of highly toxic chemical compounds that generally are organic esters of substituted phosphoric acid. Nerve agents affect body functions by inhibiting cholinesterase enzymes, permitting accumulation of acetylcholine and subsequent paralysis. Two general categories of nerve agents are currently stockpiled: G agents and V agents. The G agent used in munitions is GB (Sarin); it is a liquid under ordinary atmospheric conditions, with a relatively high vapor pressure. GB is colorless and odorless. It is readily absorbed into the body by inhalation, by ingestion, and through the skin and eyes without producing any irritation prior to onset of symptoms. It is miscible in both polar and nonpolar solvents. It hydrolyzes slowly in water at neutral or slightly acidic pH, and more rapidly under strong alkaline or acidic conditions. The hydrolysis products are significantly less toxic than the agent.

Table 1: US Chemical Warfare Munitions

Designation	Description	Fill	Explosives	Propellant	Fuze
M55	115mm Rocket	10.7 lb GB or 10.2 lb VX	3.2 lb	19.3 lb	Yes
M23	Land Mine	10.5 lb VX	0.8 lb	None	Yes
M2/M2A1	4.2" Mortar	6.0 lb H/HD	0.14 lb	0.6 lb	Yes
M60	105mm Cartridge	3.0 lb H/HD	0.26 lb	2.8 lb	Yes
M360	105mm Cartridge	1.6 lb GB	1.1 lb	2.8 lb	Yes
M110	155mm Projectile	11.7 lb H/HD	0.83 lb	None	No
M104	155mm Projectile	11.7 lb HD	0.83 lb	None	No
M121A1	155mm Projectile	6.5 lb GB or VX	2.45 lb	None	No
M122A1	155mm Projectile	6.5 lb GB	2.45 lb	None	No
M426	8" Projectile	14.5 lb GB or VX	7.0 lb	None	No
MC-1	750 lb Bomb	220 lb GB	None	None	No
MK-94	500 lb Bomb	108 lb GB	None	None	No
TC	Ton Container	1600 lb GB/VX/H	None	None	No
TMU-28	Spray Tank	1356 lb VX	None	None	No

Table 2: CW Agents: Physical & Chemical Properties

	GB	VX	HD
Chemical Name	Isoproply methyl phosphonofluoridate		Bis(2-chloro-ethyl) sulfide
Common Name	Sarin	-	Distilled Mustard
Molecular wt	140.1	267.0	159.1
Liquid Density (25°C)	1.09	1.008	1.27
Freezing point (°C)	-56°	-39°	14°
Vapor pressure at 20°C (mm Hg)	2.2	.0007	.072
Decomposition Temp (°C)	400-560	700-800	149-177
LD_{50} ($mg\text{-}min/m^3$)	100	*	1500
Chemical Formula	$CH_3P(O)(F)OCH(CH_3)_2$	$CH_3P(:O)(OC_2H_5)SC_2H_4N(iso\text{-}C_3H_7)_2$	$(ClCH_2CH)_2S$

*Exposure is primarily via skin penetration. Medium lethal dose is 2.5 mg (equivalent to 0.56 mg intravaneous dose).

The only V agent used in munitions is VX. It is amber in color and odorless. A liquid at normal ambient temperatures, it has an extremely low vapor pressure. Consequently, it is dispersed as an aerosol, and exposure is primarily via skin penetration. The toxicity of VX is 3-10 times that of GB. Exposure of either agent can result in death within minutes.

Blister agents, also called vesicants, are systemic poisons, attacking the eyes and lungs and blistering the skin with either liquid or vapor contact. Most blister agents cause little or no pain on contact. Symptoms of exposure do not usually appear for several hours. Mustard blister agents include Levinstein Mustard (H), and Distilled Mustard (HD); these are the only two mustard agents in munitions.

Pure mustard is a colorless, oily liquid; impurities impart a characteristic garlic odor. It is sufficiently volatile to be effective as a vapor in warm weather.

As was shown in Table 1, each agent can be dispersed by a variety of munitions. Figure 1 illustrates an M360 cartridge. (A projectile, burster, fuze, cartridge casing, propellant and initiator comprise a cartridge). Disposal poses significant challenges:

a. Safe disassembly of the explosives.

b. Disposal of the removed explosive components and propellants.

c. Accessing the agent cavity.

d. Disposal of the toxic agent.

e. Disposal of the munition bodies.

f. Disposal of the process generated wastes.

In addition to these considerations, DA has established criteria for the storage, transportation, and disposal of CW materiel. These criteria address the following areas, and influence selection of disposal alternatives:

a. Restrictions on total quantity of explosives within the process structure.

b. Agent emission limitations.

c. Process effluents standards.

d. Personnel safety requirements.

In September 1979, the Chemical Agent/Munitions Disposal System (CAMDS) at Tooele Army Depot, Utah, became operational. This $67M prototype plant serves as a test facility to evaluate alternate processes for possible incorporation into future large scale production CW demilitarization facilities.

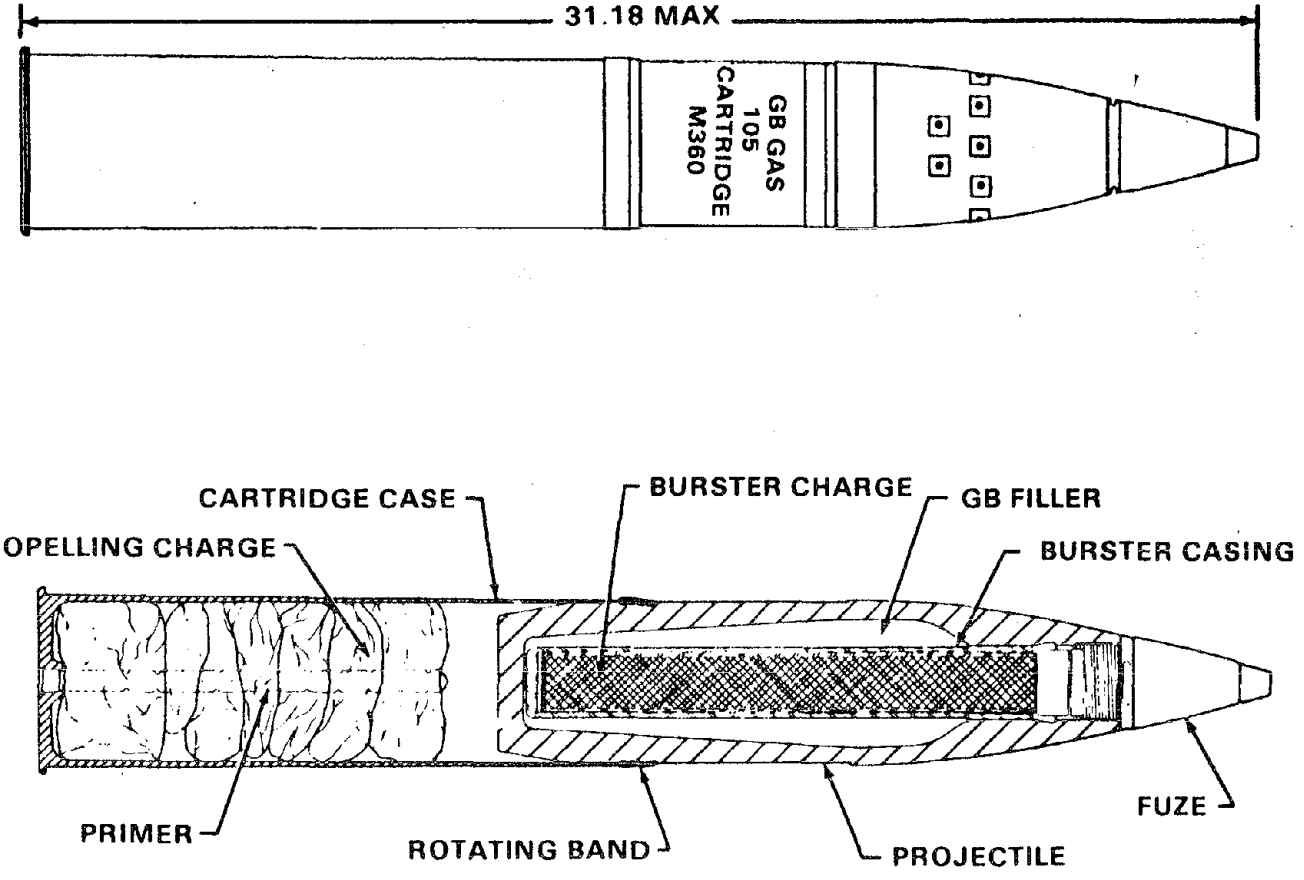

FIGURE 1: CARTRIDGE, 105 MILLIMETER: AGENT GB, M360

The first of these production facilities is currently under design; start of construction is scheduled for the summer of 1985. The facility is to be built on Johnston Island, one of four small land bodies that make up Johnston Atoll (JA), located 717 nautical miles west southwest of Honolulu, Hawaii.

JA is an unincorporated US possession under joint management by the Defense Nuclear Agency (DNA) and the Department of Interior (DOI). Johnston Island, the largest body in the Atoll, is approximately 2 miles long and 1/2 mile wide, and covers 630 acres. The Atoll is both a wildlife refuge monitored by the Fish and Wildlife Service, and a contingency site maintained by DNA for resumption of above ground nuclear testing.

The CW stocks stored at JA came originally from Okinawa in 1971 as a result of their prohibition from being returned to the United States by Public Law 91-672.

When DA gave direction in March 1981 to initiate planning for disposal of the Code H munitions on JA, environmental considerations were given priority. A public scoping meeting was held in Honolulu, HI in June 1983 and a final EIS published in November 1983. Of the viable alternatives, construction of a state-of-the-art disposal facility on JA was determined to offer the best solution. The technology selected is that being demonstrated by the CAMDS prototype facility.

The key elements of this technology are illustrated in Figure 2 and provide the basis for design of the JACADS process and facility. The site layout is shown in Figure 3.

The overriding facility criteria is agent containment. By maintaining negative pressures within the facility, agent containment is provided for all processing steps. The resulting ventilation air is scrubbed by redundant charcoal filters as illustrated in Figure 4. These filters are 99.99999% efficient in removal of agent prior to discharge of the ventilation air to the atmosphere. Containment of both the overpressure and fragments resulting from an accidental detonation is provided for those process steps involving explosively configured munitions. This total containment is accomplished by use of a reinforced concrete structure contained within the facility. Blast valves and containment dampers isolate this structure from the rest of the facility in the event of an accidental detonation.

The specific process steps and equipment required for demilitarization are a function of the munition type. Generically, all munition types fall into one of three categories:

a. Rockets and Mines. These thin-walled munitions are processed without removal of their explosive components.

b. Projectiles and Mortars. Removal of explosives from these heavy-walled munitions is the first processing step.

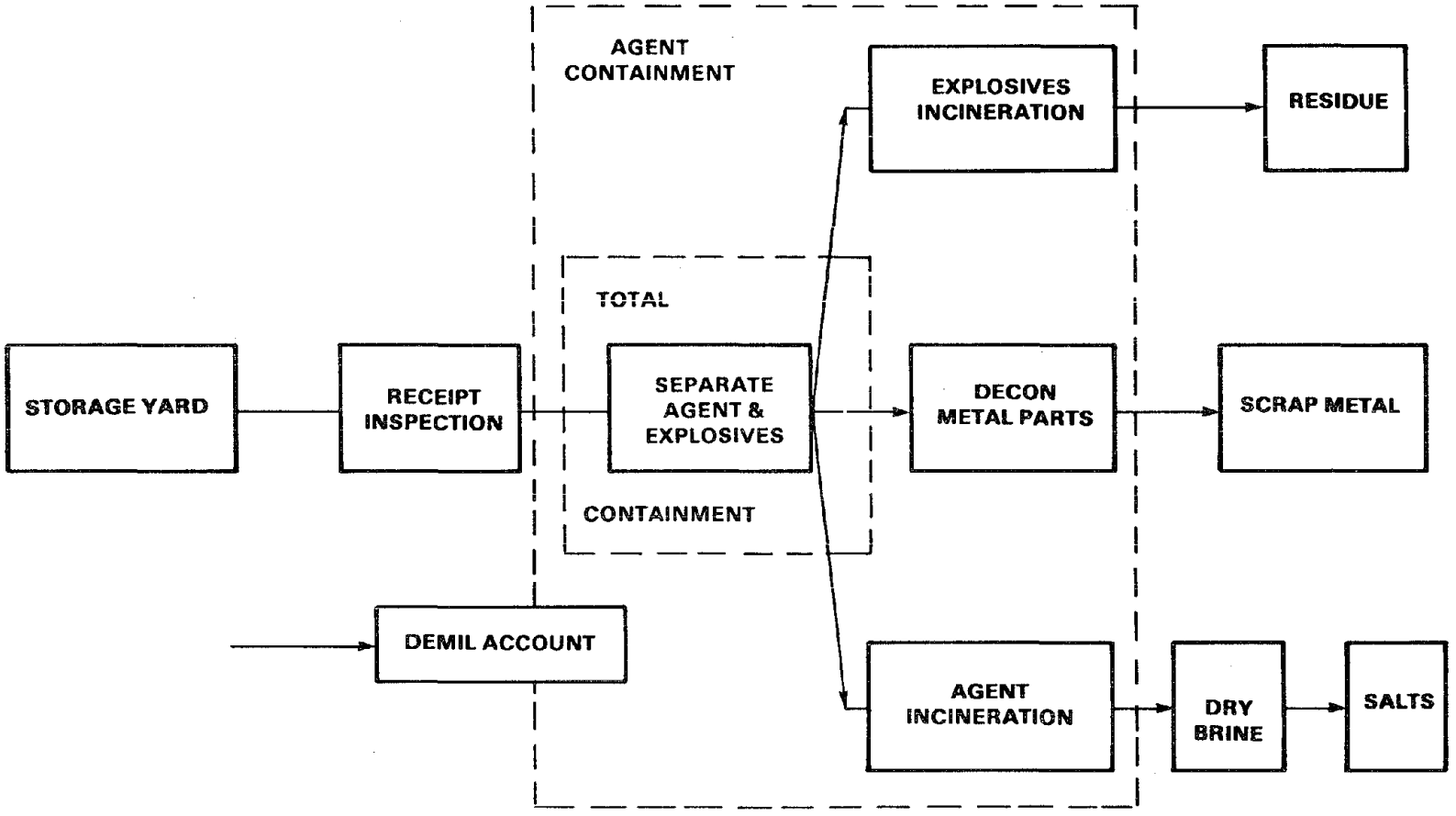

FIGURE 2: CHEMICAL MUNITION DEMILITARIZATION SCHEMATIC

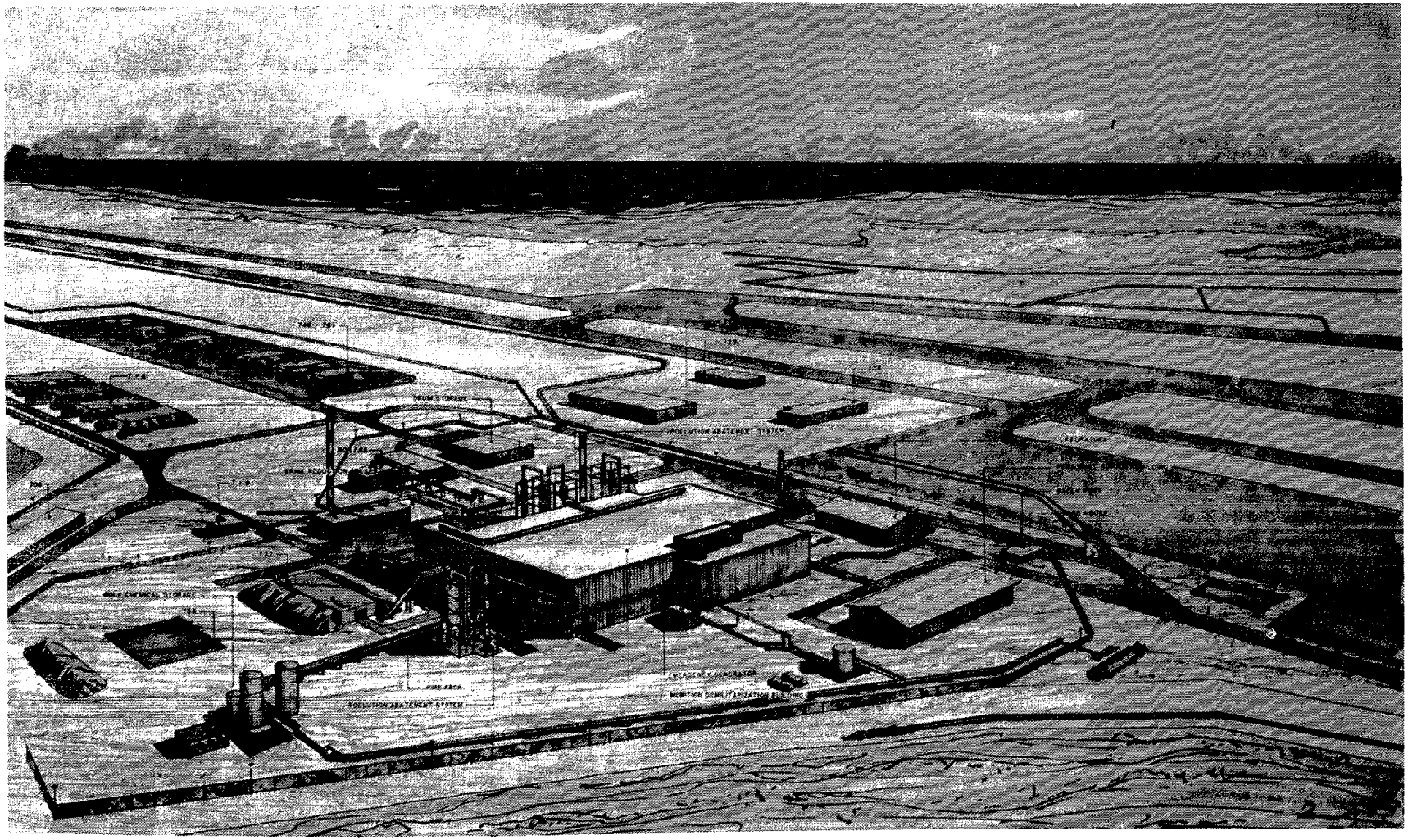

Figure 3: Perspective View of Site – Johnston Atoll
Chemical Agent Disposal System

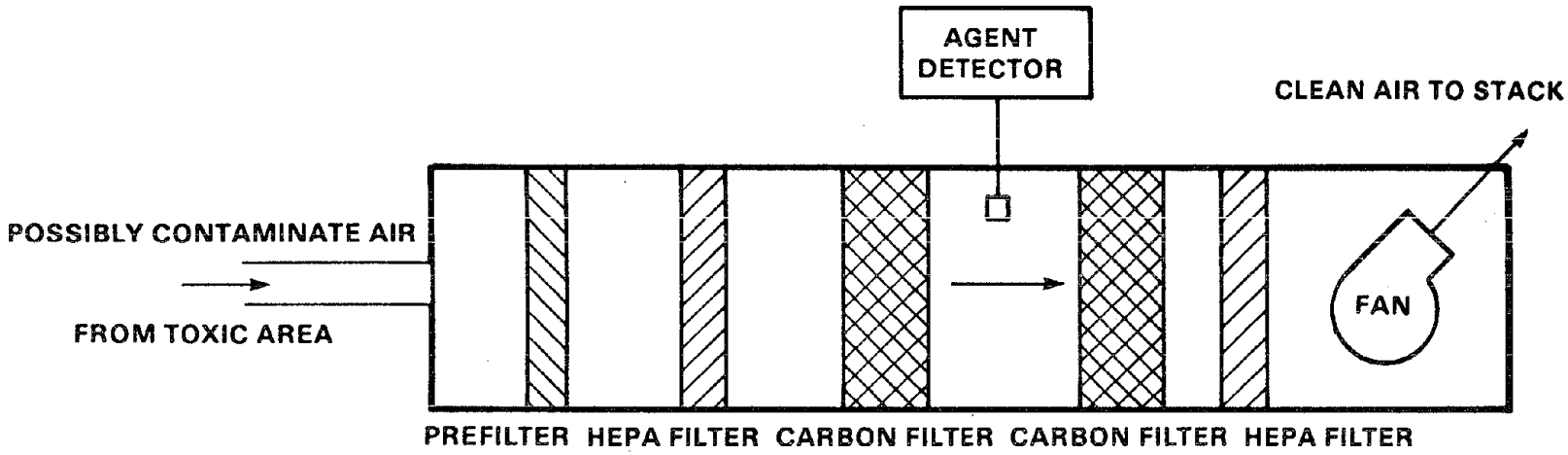

FIGURE 4: TYPICAL FILTER HOUSING LAYOUT

c. Bulk Items. This category includes bombs, spray tanks, and ton containers; they do not contain explosives in their storage configurations.

For all three munition categories, the demilitarization process involves two distinct operations: preparation for thermal treatment, followed by thermal processing; agent destruction is accomplished by incineration.

The JACADS facility has been designed with the capability to process all three munition categories. The primary process facility comprises 67,000 sq ft on two levels. The second floor houses the equipment required for preparation of the munition for thermal processing while the process's four furnaces are located on the ground level facilitating gravity feeding of munition components into the furnaces. The four process furnaces: the liquid incinerator, deactivation furnace, metal parts furnace, and dunnage incinerator, are the heart of the demilitarization operation. The following paragraphs discuss the role of each of these furnaces in the disposal operations.

Chemical agent, drained as a liquid from all munitions and pumped to intermediate holding tanks, is incinerated by the liquid incinerator.

The liquid incinerator has been designed with the capabilities shown in Table 3.

Table 3: Incineration Rates

	lbs/hr
GB	1050
VX	700
Mustard	1330
Decontamination Solutions	2000

Agent pumped from the intermediate holding tanks is atomized by a spray nozzle into the primary chamber of the two chamber furnace. The resultant combustion products are further incinerated in the secondary fume burner. The following incinerator criteria has been established for the liquid incinerator:[3].

Table 4: Agent Incinerator Criteria

	Primary Chamber	Fume Burner
Burner Zone Temperature	2500-3500°F	2500-3500°F
Secondary Zone Temperature (avg)	1800-2200°F	2000°F
Residence Time	2.0 sec	.5 sec

In the design of an agent incinerator, the overriding criteria is destruction efficiency. Table 5 illustrates the degree of destruction required for each agent.

Table 5: Agent Incinerator Destruction Requirements (200% Excess Air)

Agent	Discharge Std (mg/m^3)	Required Destruction Efficiency (%)
GB	0.0003	99.999999
VX	0.00003	99.9999999
H	0.03	99.99995

Disposal of the munitions' explosive and propellant components is accomplished by incineration. Energetic material is fed into a deactivation furnace system. Bursters and rocket propellants are preprocessed through a mechanical shear. This shear reduces the size of the material and exposes additional surface area to facilitate controlled combustion rather than detonation. Fuzes, booster pellets, and supplementary charges are fed to the furnace intact.

The deactivation furnace consists of a steel rotary retort kiln, operated at 1200°F, and a heated discharge conveyor, operated at 1000°F. Residence time of the explosives inside the retort is approximately 12 minutes - sufficient to allow complete burning of all energetic material. Upon exiting the retort, the non-combustible components travel on the heated discharge conveyor for an additional 15 minutes to insure complete thermal decontamination of any residual agent. The deactivation furnace system is capable of processing approximately 500 lbs/hr of explosives.

The exhaust of the deactivation furnace exits through a blast attenuation duct prior to entry into a secondary fume burner. The secondary fume burner has been designed to the same criteria as the liquid incinerator afterburner. The deactivation furnace room has been designed to provide containment of all fragments, overpressure and agent in the event of a detonation during the incineration process.

In addition to the agent and explosives, the munition metal parts constitutes a third category of hazardous waste. Metal which has been in contact with liquid agent has been shown to release agent vapors when subjected to elevated temperatures, even after the metal has been chemically decontaminated. For this reason, all metal parts are thermally decontaminated to a criteria of 1000°F for 15 minutes prior to discharge from the process areas. Since rockets and land mines are processed without removal of their explosives, metal parts from these munitions are decontaminated in the deactivation furnace system concurrent with incineration of the energetic material. Metal parts from projectiles, mortars, and bulk items are processed through a separate metal parts furnace system for thermal decontamination. This modified roller hearth furnace is

designed to process metal parts through the furnace on reusable 3' x 10' trays with a residence time of approximately 60 minutes. The throughput rates of this furnace are a function of the munition types, as shown in Table 6.

Table 6: Munition Peak Processing Rates

Munition Type	No./Hour	Lbs/Hour (Metal)
105	181	5800
4.2	178	3200
155	90	8100
8"	47	8700
Bombs	2.4	1200
TCs	1.66	2600
Rockets	60	-
Mines	72	-

In addition to the decontamination of metal parts, this furnace has been designed to incinerate a residual agent "heel" of 5% by weight of the agent fill of each munition. Exhaust gases from the decontamination chamber of the metal parts furnace are incinerated in a secondary fume burner.

The fourth furnace system within the demilitarization facility is the dunnage incinerator. This incinerator is designed to burn all process dunnage including agent contaminated wood, wooden pallets impregnated with PCP preservatives, contaminated protective clothing, and other packaging materials. The combustion chamber is a refractory lined incinerator operated at approximately 2000°F. A ram feed processes materials into the furnace, simultaneously discharging ash from the opposite end. A secondary fume burner assures complete incineration of all hydrocarbons. The incinerator has a throughput rate of approximately 1000 lbs/hour of combustible dunnage. Although all furnaces are fired by No. 2 fuel oil, a substantial portion of the heat input is provided by the combustion products. Table 7 shows BTU's/hr from combustion of the waste inputs.

Table 7: Incineration Combustion Rates

		BTU's/hour
Liquid Incinerator	GB	9,580,000
	VX	9,331,000
	H	9,520,000
Deactivation Furnace	Explosives	993,000
	Propellant	3,185,000
Dunnage Incinerator	Wood	8,000,000

Each furnace system has an independent pollution abatement system designed to scrub the products of combustion. Primary products of combustion are shown below.

GB: CO_2, H_2O, P_2O_5, HF

VX: NOx, P_2O_5, SO_2, CO_2, H_2O

Mustard: CO_2, SO_2, HCl, H_2O

In addition, impurities in the agents result in trace quantities of heavy metals in the furnace exhaust.

Figure 5 illustrates the basic pollution abatement system; similar systems are utilized for three of the four process furnaces. The incinerators have been designed for compliance with applicable RCRA (HCl and particulate emissions) and Clean Air Act requirements. The exhaust of the secondary fume burner is drawn through the pollution abatement system by an induced draft fan. The quench reduces the afterburner exhaust to approximately 200°F and results in adiabitic saturation of the effluent stream. Eighteen percent caustic solution is used as a quench media to assure neutralization of any acid gases condensed in the quench. The high energy venturi is a variable throat venturi with an approximate 40" WG pressure drop designed to provide 99% efficiency in removal of particulate larger than 0.5 microns. The counter-flow caustic scrubber uses stainless steel pall rings to scrub remaining acid gases. Mist eliminators are used primarily for removal of P_2O_5, but also to entrain particulate not removed by the venturi. The mist eliminators have been designed with a counterflow acid wash to prevent plugging by small particulate metal oxides.

Liquid effluent from the pollution abatement system is discarded when the specific gravity reaches 1.08 - 1.20, depending upon the agent being processed. Excess water is evaporated from this effluent yielding a waste salt suitable for landfill.

While the furnace system is the heart of the demilitarization system, the control room is the brains. With the exception of the munition input and residue removal, the demilitarization operation is totally automated and controlled from the control room.

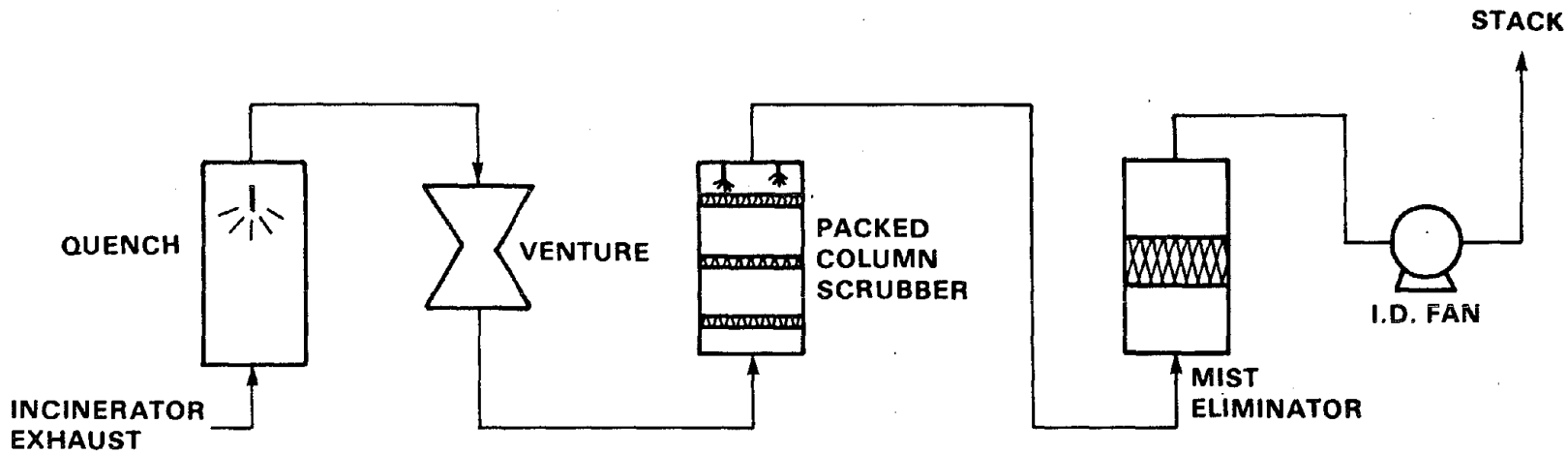

FIGURE 5: INCINERATOR POLLUTION ABATEMENT FLOW DIAGRAM

Munition processing is accomplished by machines designed and built for specific chemical demilitarization operations. This equipment includes: the Rocket Shear Machine for shearing rockets and explosives, the Projectile/Mortar Disassembly Machine for removing explosive components by reversing the assembly process, the Multipurpose Demilitarization Machine for draining agent from projectiles and mortars, and the Bulk Drain Station for punching and draining bombs, ton containers, and spray tanks. Robots are used for munition handling within the process area. Process information is continually fed to the control room for computer analysis. The control room operators are provided with closed circuit television to facilitate monitoring of the process flow. Additionally, observation corridors surround the process area, allowing for direct viewing of these areas, if needed.

Although the demilitarization equipment has been designed to preclude the requirement for operators in the process area, personnel entry is required to affect maintenance or repairs. Maintenance personnel entering agent process areas are protected from exposure to chemical agents by the Demilitarization Protective Ensemble shown in Figure 6. This air supplied protective suit was developed specifically for chemical demilitarization operations. In addition to the air supply umbillical, the suit is provided with a backup self-contained respirator for emergency egress in the event of a loss of supply air.

In use, the worker is heat-sealed into the disposable chlorinated polyethelene suit and a helium leak test is performed to insure a complete seal. Personnel entry into toxic areas requires at least two individuals and visual contact must be maintained betwen the workers in any one area. Each worker in the protective ensemble can communicate with the control room and other personnel via an RF communications system.

Normal clothing for workers in the noncontaminated areas of the facility is cotton coveralls. Each worker carries a protective gas mask which can be donned in the event of an agent alarm or process upset. The differential pressures within the facility have been designed to prevent migration of agent into noncontaminated work areas. These differential room pressures are constantly monitored by the control room.

All work areas, the control room, and furnace and filter exhausts are continually monitored for agent during operations. The primary agent monitor used is the Automated Continuous Agent Monitoring System (ACAMS) developed for demilitarization operations. The ACAMS is an on-line automated gas chromatograph capable of specific identification of the chemical agents at concentrations less than the allowable work area limits established by the DA Surgeon General as listed in Table 8.

Table 8: Allowable Work Area Concentrations (Time Weighted Average)

GB	.0001 mg/m^3
VX	.00001 mg/m^3
H	.003 mg/m^3

Figure 7: Demilitarization Protective Ensemble

As shown in Figure 7, the ACAMS includes a preconcentration tube, a GC column, and a flame photometric detector. In operation, sample air is drawn through the preconcentrator tube for a predetermined period. At the end of this period the sampling is interrupted and the preconcentrator tube is heated. A counter-flow carrier gas desorbs any agent accumulated in the preconcentrator. The desorbed sample is drawn through a Gas Chromatograph column designed to separate the sample constituants prior to introduction into the flame photometeric detector. The ACAMS is controlled by an internal microprocessor and provides both an analog and digital output. The output is displayed locally as well as transmitted to the control room.

Data from the air monitors provide a permanent record of plant emissions as well as a record of the potential for exposure of personnel to agents. Additionally, routine medical examination of plant personnel is used to monitor indications of agent exposure.

Subsequent to the termination of ocean disposal in 1970, the Army has disposed of over 15,000,000 pounds of CW agents, The procedures and equipment developed and being implemented by the Army have demonstrated that disposal of even the most hazardous waste can be accomplished safety with minimal impact to the environment.

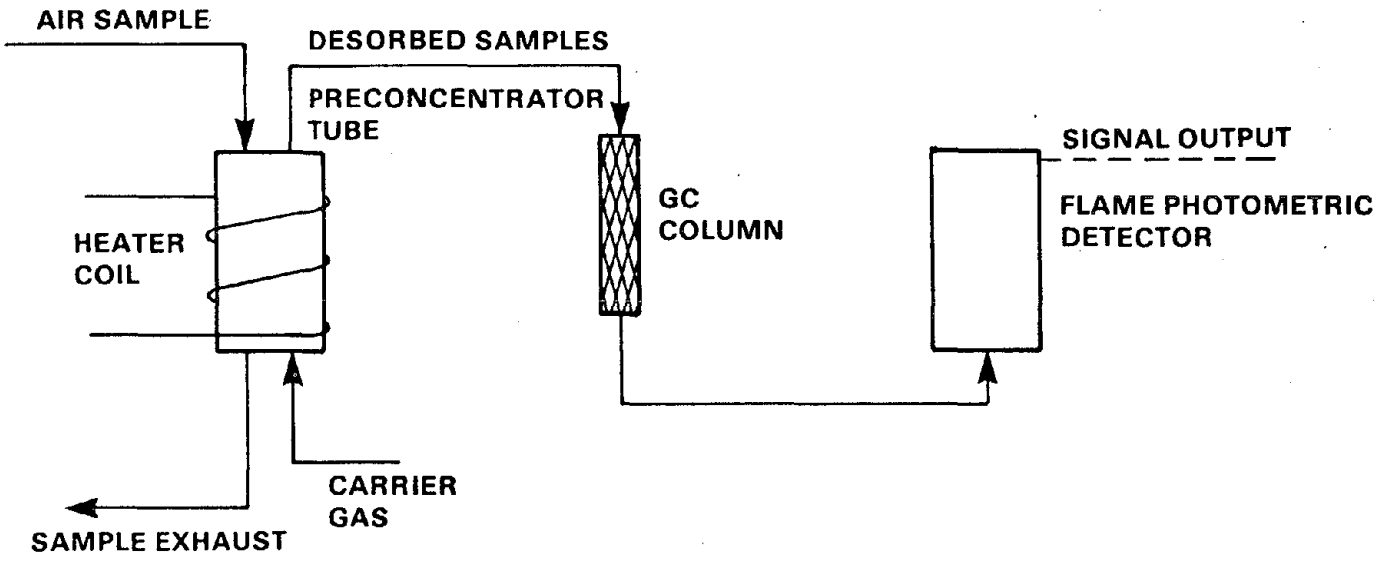

FIGURE 7: SCHEMATIC OF AUTOMATED CONTINUOUS AGENT MONITORING SYSTEM (ACAMS)

REFERENCES

1. "Banning Chemical Weapons", by Richard L. Wagner, Jr. and Theodore S. Gold, Defense 84, June 1984. pp 22-32.

2. Report of the Disposal Hazards of Certain Chemical Warfare Agents and Munitions, prepared by an Ad Hoc Advisory Committee of the National Academy of Sciences, Washington, DC. June 24, 1969.

3. Technical Paper Defining the Operating Conditions for the Incineration of the Chemical Agents GB, H, and VX, 7 May 1984; US Army Toxic and Hazardous Materials Agency.